Popular Summary

Factors Affecting the Evolution of Hurricane Erin and the

Distributions of Hydrometeors: Role of Microphysical Processes

by

Greg M. McFarquhar, Henian Zhang, Jimy Dudhia, Jeffrey B. Halverson

Gerald Heymsfield, Robbie Hood, and Frank Marks Jr.

Fine-resolution simulations of Hurricane Erin 2001 are conducted using the Penn State University/National Center for Atmospheric Research mesoscale model version 3.5 to investigate the role of thermodynamic, boundary layer and microphysical processes in Erin's growth and maintenance, and their effects on the horizontal and vertical distributions of hydrometeors. Through comparison against radar, radiometer, and dropsonde data collected during the Convection and Moisture Experiment 4, it is seen that realistic simulations of Erin are obtained provided that fine resolution simulations with detailed representations of physical processes are conducted.

The principle findings of the study are as follows: 1) a new iterative condensation scheme, which limits the unphysical increase of equivalent potential temperature associated with most condensation schemes, increases the horizontal size of the hurricane, decreases its maximum rainfall rate, reduces its intensity, and makes its eye more moist; 2) in general, microphysical parameterization schemes with more categories of hydrometeors produce more intense hurricanes, larger hydrometeor mixing ratios, and more intense updrafts and downdrafts; 3) the choice of coefficients describing hydrometeor fall velocities has as big of an impact on the hurricane simulations as does choice of microphysical parameterization scheme with no clear relationship between fall velocity and hurricane intensity; and 4) in order for a tropical cyclone to adequately intensify, an advanced boundary layer scheme (e.g., Burk-Thompson scheme) must be

used to represent boundary layer processes. The impacts of varying simulations on the horizontal and vertical distributions of different categories of hydrometeor species, on equivalent potential temperature, and on storm updrafts and downdrafts are examined to determine how the release of latent heat feedbacks upon the structure of Erin. In general, all simulations tend to overpredict precipitation rate and hydrometeor mixing ratios. The ramifications of these findings for quantitative precipitation forecasts (QPFs) of tropical cyclones are discussed.

Factors Affecting the Evolution of Hurricane Erin and the Distributions of Hydrometeors: Role of Microphysical Processes

by

Greg M. McFarquhar[1], Henian Zhang[1], Jimy Dudhia[2], Jeffrey B. Halverson[3]

Gerald Heymsfield[3], Robbie Hood[4], and Frank Marks Jr.[5]

[1]Dept. of Atmospheric Sciences, University of Illinois, Urbana, IL

[2]National Center for Atmospheric Research, Boulder, CO

[3]NASA Goddard, Greenbelt, MD

[4]NASA Huntsville, Huntsville, AL

[5]NOAA HRD, Miami, FL

Submit to *J. Atmos. Sci.*

30 June 2003

Corresponding Author: Prof. Greg M. McFarquhar, Dept. of Atmospheric Sciences, University of Illinios, 105 S. Gregory Street, Urbana, IL 61801 mcfarq@atmos.uiuc.edu

Abstract

Fine-resolution simulations of Hurricane Erin 2001 are conducted using the Penn State University/National Center for Atmospheric Research mesoscale model version 3.5 to investigate the role of thermodynamic, boundary layer and microphysical processes in Erin's growth and maintenance, and their effects on the horizontal and vertical distributions of hydrometeors. Through comparison against radar, radiometer, and dropsonde data collected during the Convection and Moisture Experiment 4, it is seen that realistic simulations of Erin are obtained provided that fine resolution simulations with detailed representations of physical processes are conducted.

The principle findings of the study are as follows: 1) a new iterative condensation scheme, which limits the unphysical increase of equivalent potential temperature associated with most condensation schemes, increases the horizontal size of the hurricane, decreases its maximum rainfall rate, reduces its intensity, and makes its eye more moist; 2) in general, microphysical parameterization schemes with more categories of hydrometeors produce more intense hurricanes, larger hydrometeor mixing ratios, and more intense updrafts and downdrafts; 3) the choice of coefficients describing hydrometeor fall velocities has as big of an impact on the hurricane simulations as does choice of microphysical parameterization scheme with no clear relationship between fall velocity and hurricane intensity; and 4) in order for a tropical cyclone to adequately intensify, an advanced boundary layer scheme (e.g., Burk-Thompson scheme) must be used to represent boundary layer processes. The impacts of varying simulations on the horizontal and vertical distributions of different categories of hydrometeor species, on equivalent potential temperature, and on storm updrafts and downdrafts are examined to

(MM5) version 3.5, are used to examine the impact of boundary-layer, and microphysical parameterization schemes on the growth and maintenance of Erin. Impacts of varying specific microphysical parameters, such as coefficients describing the fall velocities of graupel particles, on hurricane dynamics are described. A new iterative condensation scheme, developed here to limit the artificial increase of equivalent potential temperature Θe that occurs during the adjustment step of many condensation schemes (Bryan and Fritsch 2000) is also tested.

Observations made during CAMEX4 provide a framework for interpretation of model results, and give information about which parameterization schemes best represent processes occurring within Erin. Radar reflectivity, estimated from the Tropical Rainfall Measuring Mission (TRMM) precipitation radar (PR), is compared against reflectivity obtained from the simulations. Vertical profiles of radar reflectivity and Doppler velocity, obtained from the ER-2 Doppler radar (Heymsfield et al. 1996), hereafter EDOP, and estimated locations of rain, cloud, and graupel retrieved from the Advanced Microwave Radiometer (Spencer et al.1994), hereafter AMPR, are also compared against the simulations. Temperature and moisture profiles obtained from dropsondes released in the hurricane eye also compared against the simulations to improve the understanding of eye thermodynamics.

The remainder of this paper is organized as follows. Section 2 provides information on the structure and evolution of Erin based on observations acquired during CAMEX-4, concentrating on those observations that are used to assess the simulations and sensitivity studies outlined in Section 3. Section 4 describes the results of the simulations and the impacts of microphysical, thermodynamic and boundary layer

that simulations were more strongly influenced by differences in descriptive microphysical parameters (e.g., size distribution intercept parameter and particle density) than by differences in the way the microphysical processes were treated in each of the ice schemes. They suggested that the application of bulk ice microphysics in cloud models might be case specific, indicating that microphysical sensitivity studies for other cloud systems may not apply to tropical cyclones. Braun and Tao (2000) also changed values of descriptive parameters in the Goddard microphysical scheme to more closely match those values that might be expected in hurricanes.

Other studies have focused on how initial conditions, data assimilation schemes, and parameterizations of other processes affect simulations of tropical cyclones, examining rainfall assimilation and cumulus parameterization schemes (Karyampudi et al. 1998), boundary layer schemes (Braun and Tao 2000), and the role of a gradient of angular momentum above regions of maximum convective heating (Krishnamurti et al. 1998). Simulations with high resolution (Liu et al. 1997, 1999) have shown that track, intensity and the inner-core structures of Hurricane Andrew could be reproduced using realistic model physics and proper initial vortices. Hence, uncertainties associated with microphysics must be placed in the context of uncertainties in the representations of other processes. Liu et al. (1997) also suggested that axisymmetric models did not adequately represent storm-environment interactions, showing that previous microphysical sensitivity studies using axisymmetric models might not be applicable.

In this paper, simulations of Hurricane Erin 2001, observed during the Convection and Moisture Experiment 4 (CAMEX4) conducted using the Pennsylvania State University/National Center for Atmospheric Research mesoscale modeling system

1. Introduction

Quantitative precipitation forecasts (QPFs) require knowledge of synoptic, mesoscale, and microscale processes, and an adequate representation of these processes in models. To improve QPFs for tropical cyclones, improved knowledge of cloud microphysical, thermodynamic and turbulent processes, land-surface-atmosphere interactions, improved measurements of atmospheric water vapor, a better understanding of mesoscale dynamics, and further development of mesoscale numerical models and cumulus parameterization schemes are required. Although several studies have investigated the influence of many such processes on the evolution of tropical cyclones, fewer recent studies have examined the impact, if any, of cloud microphysical processes on the structure and evolution of these systems and on the QPFs for these storms.

Previous studies have shown that representations of microphysical processes affect simulations of tropical cyclones. Willoughby et al. (1984) showed that hurricane simulations with parameterized ice microphysics had very different structures and evolution compared to those with liquid water microphysics. Lord et al. (1984) and Lord and Lord (1988) used an axisymmetric, nonhydrostatic model to show that the cooling associated with melting ice particles initiates and maintains model downdrafts, the extent and intensity of which are determined by the horizontal advection of hydrometeors from the convection, together with the fallspeeds of snow and graupel and the conversion rates between hydrometeor species. These downdrafts contribute to the formation of multiple convective rings, which in turn modifies the development of the storm (Willoughby et al. 1984). McCumber et al. (1991) also evaluated the performance of several ice parameterizations in both tropical squall-type and non-squall type systems, concluding

determine how the release of latent heat feedbacks upon the structure of Erin. In general, all simulations tend to overpredict precipitation rate and hydrometeor mixing ratios. The ramifications of these findings for quantitative precipitation forecasts (QPFs) of tropical cyclones are discussed.

processes on the structure and evolution of Erin. The significance of the results are summarized in Section 5.

2. Observations of Hurricane Erin

Hurricane Erin (2001) was the first tropical cyclone to reach hurricane status in 2001 and achieved maximum wind speeds of approximately 190 km h^{-1}. Pasch and Brown (2002) report that Erin formed from a tropical wave emerging over west Africa, and weakened and strengthened a number of times before regaining tropical storm strength on 7 September 2001. After brushing Bermuda on 9 September, Erin moved to the north-northwest and weakened slower than typical storms. Erin reached category 3 on the Saffir-Simpson scale, and never achieved landfall. Erin is a good candidate for studies on microphysical effects on storm evolution because additional unknowns about impacts of landfall are avoided. Observations of Erin are plentiful. During CAMEX4, the NOAA P-3 and the NASA ER-2 and DC-8 flew in coordination, obtaining comprehensive data on the wind, temperature, and moisture structure of the storm during its mature phase on 10 September 2001.

Although no rainfall gauge measurements exist from Erin, information about hydrometeor distributions can be obtained from satellite and airborne remote sensing. Algorithms exist to convert radar reflectivity, Z, to rainfall rate, R, but direct comparisons of modeled and observed Z are performed here to avoid uncertainties associated with Z-R relations. Figure 1 and Figure 2 show examples of radar images of Erin on September 10, 2001 from two separate sweeps made during the first and second penetration of the NOAA P-3 into Erin at 181154 and 191446 UTC respectively. The observations were made during the mature stage of Erin, critical for studying feedbacks of microphysical

processes on dynamics. Depending on the threshold reflectivity used to define the eye and depending on time, the width of the eye varies between 30 and 60 km in diameter, with the diameter sometimes hard to define given the clear wave asymmetry that is seen in the reflectivity of the inner eye wall. This clear wave asymmetry rotates counter clockwise during the time period of the simulation, being to the south of the eye in Fig. 1 and to the west of the eye in Fig. 2; Marks et al. (2003) further characterize this eye wall asymmetry and hypothesize causes for its existence. Other asymmetries in the reflectivity pattern are also noted, with the rain bands of maximum reflectivity to the north and east of the eye in Fig. 1 and to the west and south of the eye in Fig. 2. The maximum Z for Erin at the time of these observations is approximately 43 dBZ, and the diameter of Erin is about 360 km. The spacing, width, and length of the asymmetrical rainbands can vary with time, but typical values are on the order of 20 km for spacings, 10 km for width, and 50 km for length. From the TRMM radar, maximum Z values measured by the PR were around 50 dBZ at 2100 UTC on 10 Septebmer. Using the 2B31 combined PR/TRMM microwave imager (TMI) retrieval algorithm, this maximum Z corresponds to a rainfall rate of approximately 100 mm h^{-1}. Although it would be impossible to expect exact replication of these results from the numerical models, similar values of reflectivity, rain rate, and similar characterizations of asymmetries should be obtained if the simulations are adequately capturing the physical processes occurring within hurricanes.

Figure 3 shows brightness temperatures (T_b) at frequencies of 10.7, 19.35, 37.1, and 85.5 GHz observed by the AMPR during a flight leg over the eye of Erin between 191946 and 193628 UTC. Combined with results of radiative transfer codes, these data give information about the presence or absence of various categories of hydrometeors.

The eye is clearly seen from radiometrically colder T_b at 10.7, 19.35, and 37.1 GHz; at 85.5 GHz, significant water vapor emission causes the clear ocean to have a relatively high T_b. Lower T_b near the eye's center compared to regions closer to the eyewall suggests significant drying, and hence less water vapor emission occurs near the center. By comparing similar AMPR images for other transects over the eye of Erin, the eye is seen to move to the northeast at approximately 30 km h^{-1} during the 3 h time period (164859 to 195030 UTC) of the AMPR observations (figures not shown). The diameter of the eye is estimated to be 37 km, similar to that estimated with the P-3 radar. The horizontal dimension is approximately 400 km, determined by looking at emissions in the lower 3 frequency channels and scattering at the highest frequency.

The 19.35 GHz channel saturates due to rain emission between 66°W and 66.5°W and for smaller areas around the eye wall at 65.7°W and 65.2°W, whereas the 10.7 GHz channel saturates for only minimal area between 66°W and 66.5°W. Based on the modeling results of Smith et al. (1994), this suggests minimal areas have rain rates greater than 30 mm h^{-1}. As with the radar and satellite data, heavier rain is required on the west side of the storm to explain these observations. Following Spencer et al. (1983), the higher frequency channels are examined for scattering effects due to ice hydrometeors. At 37.1 GHz, a blue region at 65.8°W between rain bands may be associated with either scattering due to graupel-size ice, or due to absence of significant thermal emission from rain or clouds. Effects of scattering due to smaller ice particles suspended within anvils are noted between 66°W and 66.5°W for the 85.5 GHz channel, and just outside the eyewall at 36°N 65.7°W and at 64.9°W. A lot of scattering from ice clouds is also noted between 64 and 64.5°W. The eyewall appears thicker at progressively higher frequencies

due to the inclusion of emissions from hydrometeor species in addition to the rain. Scattering from ice in a relatively narrow band of 10 to 20 km from ice clouds is also seen near the locations of the eyewall at 65 and 65.7°W. In general, the scattering effects at the 37.1 and 85.5 GHz channels are substantially less than those associated with a squall line over the Gulf of Mexico noted by Spencer et al. (1994), and do not require large amounts of graupel-size ice to explain them.

Analysis of data collected by EDOP during similar transects provides vertical profiles of velocity and Z within the storm. Figure 4 shows Z and Doppler velocity, a combination of ambient velocity and particle fall speed, for the time period shown in Fig. 3. The orientation of Fig. 4 is different from Fig. 3; points to the right of the eye occur at later times and hence are to the west. To the west of the approximately 40 km wide eye, precipitation and rain bands are more intense and a large region of precipitation of varying intensities about 46 km wide is seen, much broader than the inner eyewall, which is only 7 km wide. This relationship is also true to the east where both the eye wall and outer layers are less intense and broad. Ice particles, extending as high as 10 km, are noted above the rainbands. On the west side, these anvils extend about 250 km behind the eye and about 80 km behind the rain bands producing them. On the east, a similar anvil extends 180 km from the eye and 65 km behind the convection producing it. A bright band is frequently noted about 4.5 km above the surface. Considerable small-scale structure is noted at all levels in the observations. There is no substantial tilting of eye walls from the center for this transect. However, for an earlier transect flown from the southwest to the northeast, significant tilting was noticed on the northeast side of the eye.

Tilting is indicative of a sheared environment that can cause a significant weakening of the storm, and may explain the weaker rain bands on the north east side of the storm.

The increase in Doppler velocities below the bright band compared to that above is associated with an increase in particle fall speed as snow particles melt to raindrops. Since the updraft regions have Z of approximately 30 dBZ, this corresponds to fall speeds on the order of 1 to 2 m s^{-1}, (Orr and Kropfli 1993), indicating that the updraft may be on the order of 5 m s^{-1}. Similar analysis was performed for EDOP data obtained from other transects over Erin, and provide valuable information for comparing with simulation results.

Dropsondes released from the ER-2 over the eye give the first set of tropospheric water vapor measurements in the upper regions of the hurricane eye (Halverson et al. 2003). The dropsonde instruments measure temperature within ±0.2°C, and moisture and wind speeds within 2%. Figure 5 shows an example of the temperature moisture profile in the eye, from a launch at 192840 UTC. Substantial drying and extremely low humidity are noted between 800 and 250 mbar, with dew point depressions between 15 and 30°C, much larger than for the ambient environment sampled through other dropsonde releases. Weak horizontal winds of approximately 10 m s^{-1} are also noted. These observations are consistent with Willoughby's (1998) hypothesis that air above the inversion has remained in the eye since the eyewall formed, and mixing with the surrounding cloud preventing the dew point depressions from dropping to 100°C that would otherwise be expected.

The above data provide information about cloud macrophysical (heights, horizontal dimensions, eye sizes), microphysical (Z, R, and information on hydrometeor types), thermodynamic (vertical profiles of temperature and moisture), and dynamic

properties (e.g., Doppler velocities) that should be replicated by hurricane simulations. The properties include small amounts of graupel aloft, small areas having R greater than 30 mm h^{-1}, maximum reflectivities of approximately 45 dBZ, a deep dry layer in the eye, highly asymmetric and variable distributions of precipitation, updrafts on the order of 5 m s^{-1}, eye dimensions of 30-40 km, and horizontal dimensions on the order of 400 km.

3. Model Simulations

A series of numerical simulations of Hurricane Erin were conducted using MM5 (Grell et al. 1995), a limited-area, nonhydrostatic, terrain-following sigma-coordinate model designed to simulate or predict mesoscale and regional-scale atmospheric circulation. Simulations describe a 4-day period from 0000 UTC on 7 September 2001 to 0000 UTC on 11 September 2001. During this time, the low pressure dropped from 1012 mbar to 968 mbar (at 1800 UTC on 9 September 2001), and then rose back to 970 mbar (Pasch and Brown 2002). Figure 6 shows the course and fine-mesh domains used for the base simulation, consisting of 112 by 112 grid points in x, y with a grid spacing of 54 km. Higher resolution simulations were performed for three finer grids of 18, 6, and 2 km and all domains had two-way nesting except for the course domain. Because of computational expense, the finer resolution domains were used only when the cyclone had started to intensify, with the 6 km domain initialized at 1200 UTC on 9 September and the 2 km domain initialized at 0000 UTC on 10 September. There are 36 uneven terrain-following σ levels or 35 half σ levels in the vertical for the base simulation, with the surface pressure and 20 mbar being the pressures at the surface and model top respectively. The innermost domain was moved 3 to 4 times, depending upon the simulation, to keep the eye of the hurricane nearly centered in the fine domain.

Global analyses fields, including temperature, relative humidity, geopotential height, and winds, from the National Center for Environmental Prediction (NCEP) global tropospheric analyses on 1° by 1° grids were used for the initial and boundary conditions. Analyses products were interpolated to the model grid points and model σ levels. Starting the simulations at a later time with a bogus vortex did not produce modeled minimum pressures that compared as well with the observations as did the above base simulation. In addition, the use of analysis nudging at model boundaries in a four-dimensional data assimilation scheme did not produce significant improvements in modeled track and minimum pressure since there was no sounding available at the initial time. Simulations that started at other times or that used global analyses from the European Centre for Medium-Range Weather Forecasts did not give as good of agreement with observations and sometimes it was very difficult to get a tropical storm to intensify under such conditions. Although reasons for differences between such simulations are no doubt important, these issues are not investigated here in order to concentrate on model sensitivities to parameterized processes.

A major goal of this study is to investigate the role of thermodynamic, boundary layer and microphysical processes in the growth and maintenance of a tropical cyclone, and to determine their effects on QPFs and the horizontal and vertical distribution of hydrometeors. Therefore, a series of simulations are conducted with varying boundary layer schemes, microphysical, and thermodynamic schemes. Table 1 summarizes the experiments designed to represent these sensitivities. Although simulations were conducted at a variety of different horizontal and vertical resolutions and with varying cumulus parameterization schemes, only the results of fine resolution simulations with

explicit microphysics are reported here; the findings are necessarily resolution dependent since many parameterization schemes are designed for, and only work adequately, for certain ranges of model resolutions. All simulations involve application of preexisting parameterization schemes, with two exceptions listed below.

The thermodynamic test involves the use of a new iterative condensation scheme, described in the Appendix, which limits the unphysical increase of Θe associated with many existing schemes. The development of this scheme was motivated by Bryan and Fritsch (2000), who determined that unphysically high values of Θ_e were predicted in numerical models for rapidly growing updrafts because of the manner in which time integration is performed and because of the way condensation is treated. The Appendix describes this new scheme whereby the artificial increase in temperature and moisture, causing the increase in Θ_e, is limited.

Another series of simulations examines the dependence of simulations on descriptive microphysical parameters, and in particular on the coefficients used to describe graupel fall speeds. The role of graupel is focused upon due to the importance of graupel conversion processes in latent heat release and storm dynamics (e.g., Lord and Lord 1988) and because mesoscale models are believed to overpredict graupel mixing ratios in hurricanes. McFarquhar and Black (2003) identified a range of a/b coefficients, where $V=aD^b$, that might apply to graupel. From their Fig. 3, coefficients corresponding to faster and slower falling graupel are used in this sensitivity study. The subsequent section describes the results of the modeling simulations, placing uncertainties associated with the used of microphysics in the context of uncertainties associated with the other parameters.

4. Model Results

a. Overview

The analysis described here concentrates on how different microphysical, thermodynamic, and boundary layer processes affect horizontal and vertical distributions of hydrometeors, precipitation amounts, and vertical motions. Subsequent papers will deal with other important issues, such as how shear affects the maintenance and evolution of Erin, how storm initialization and resolution affects results, and influences due to other dynamical processes. For all simulations here, CAMEX4 observations are used to assess the adequacy of model assumptions. However, no "right" simulation is found, the purpose of this study is principally to determine influences of various processes on the growth and maintenance of Erin.

The simulated tracks of Erin do not vary substantially for the simulations discussed below and described in Table 1. One example of a simulated track is shown in Fig. 6, and all simulated tracks were consistently west of the observed track, with the degree of variation from the observed track varying somewhat. Simulations with different domains, large-scale forcings, and initialization times failed to yield better tracks that also produced reasonable strength hurricanes. Because different physical processes had substantial impacts on the intensification of the hurricane, the distribution and type of condensate, and on the inner eye thermodynamics for a given large-scale forcing, as discussed below, this suggests that the large-scale forcing, and not these physical processes, are most responsible for determining the track.

b. Predicted Sea-Level Pressures and Surface Winds

The different lines in Figure 7 show the temporal evolution of minimum sea-level pressure and maximum surface wind speed for simulations with a 2 km inner grid using the Burk-Thompson boundary layer scheme, the Betts-Miller convective scheme for the course domains, and a variety of microphysical parameterization schemes. The lines in Figure 8 represent similar simulations except that the Eta scheme is used to characterize boundary layer processes; there is no simulation with the Reisner graupel scheme for this case because some instability prevented a solution. The solid line represents observations. The simulations characterize well the evolution and structure of the system, albeit with a quicker intensification. For the Eta simulations, there is larger variation between microphysical schemes in how quickly Erin intensifies and in the minimum sea-level pressure realized compared to the Burk-Thompson simulations, especially if the Reisner graupel scheme in Fig. 7 is ignored. This shows there is no simple relationship between use of schemes and the intensity of the cyclone. However, some general trends can still be noted between microphysical schemes.

The microphysical schemes differ in their complexity and in how many hydrometeor species are included. The simple ice scheme of Dudhia (1989), which allows only ice above the melting layer and water below, is less detailed than the Reisner et al. (1996) mixed-phase scheme, which allows ice and snow, but no graupel or riming processes. The Goddard microphysics scheme (Lin et al. 1983; Tao and Simpson 1993) and the Reisner et al. (1998) graupel scheme add additional equations for prediction of graupel. In general, as more details and species are included, Erin intensifies to lower pressures and greater surface winds; for example, the use of multiple hydrometeors in Reisner graupel scheme gives lower central pressure in Fig. 7, and simple ice scheme

gives higher central pressure in Fig. 8. It is possible that increased estimates of latent heat associated with hydrometeor conversions occurring in more complex schemes lead to lower pressures, faster winds, and more evaporative cooling maintaining a deeper hurricane. However, many feedbacks force schemes to work differently relative to each other depending on representations of other processes, such as boundary layer processes.

Previous studies for mid-latitude cyclones (McCumber et al. 1991) have shown that not only does the choice of microphysics scheme affect results, but also the choice of descriptive microphysical parameters, such as the intercept parameter of size distributions and the representation of hydrometeor fall velocity. Figure 9 shows minimum pressure and maximum winds derived from three simulations with varying representations of graupel fall velocity. Note that these representations of graupel fall velocity were all identified as being plausible based on catalogs of past observations derived by McFarquhar and Black (2003). The results for the different simulations start to diverge for time periods when the fine domain simulations are initialized (D3 and D4). For this choice of base conditions, simulations with greater fall speeds produce more intense hurricanes and greater wind speeds. The range of variation between minimum pressure, 6 mbar, and maximum surface wind speeds, 5 m s^{-1}, is comparable to variations between microphysics schemes. Because various microphysical schemes may have different descriptive microphysical parameters, it is hard to decouple effects associated with varying schemes and microphysical parameters. Nevertheless, Fig. 9 shows that careful choice of descriptive parameters must be made in order to have reasonable hurricane simulations. This may be especially problematic since McFarquhar and Black (2003)

have shown that many microphysical parameterizations, designed for mid-latitude clouds, might not be applicable to tropical cyclones.

To place uncertainties associated with representations of microphysical processes in context, impacts of varying representations of other physical processes are examined. Figure 10 shows how the representation of the boundary layer affects the intensity and maximum wind speeds of Erin, all simulations conducted with Goddard microphysics. Although the schemes initially give similar results, they rapidly diverge later, especially when the fine domains are initialized. Differences between boundary layer simulations are greater than those between microphysics simulations, with minimum center pressures varying by over 20 mbar and maximum winds by up to 10 m s^{-1}, compared to differences of 14 mbar and 5 m s^{-1} for microphysics. The Burk-Thompson scheme, a local scheme allowing for mixing between layers based on prediction of turbulent kinetic energy, compares best against observations for this combination of parameterizations. In general, the Blackadar scheme produces a higher pressure than the other schemes because excessively deep vertical mixing acts to dry the lower boundary layer and reduce the hurricane intensity (Braun and Tao 2000).

The final simulation series looked at how a new representation of condensation affected hurricane evolution, and to see if potential overestimates of heating and moisture associated with conventional schemes provide artificial warming, condensate production, and increased updrafts to the degree that occurs in simulations of vigorous thunderstorms (Bryan and Fritsch 2000). Figure 11 shows the impact of the new condensation scheme on the minimum pressure and surface winds for simulations conducted with the Burk-Thompson boundary and Reisner et al. mixed-phase scheme. A higher minimum surface

pressure of up to 8 mbar and a lower maximum surface wind of up to 5 m s^{-1} are realized, uncertainties comparable to those associated with representations of microphysical processes. For simulations conducted with the Eta boundary layer scheme (not shown), the differences in minimum surface pressure and maximum surface wind were even greater (up to 12 mbar and 6 m s^{-1} respectively). The new scheme reduces the increase of latent heat because there is not as much condensation, and this, combined with the lower surface winds, acts to limit the evaporation from the ocean surface and hence the intensification of the low pressure.

The results presented in this subsection show that, although the choice of microphysical parameterization scheme affects the intensification of the hurricane, there are multiple processes that must also be considered in order to accurately predict the intensification of the hurricane. There is no easy interpretation of results or choice of "correct" parameterization scheme as the microphysical scheme that produces results closest to observations for one boundary layer scheme, may not produce results closer to observations for another parameterization scheme. Further, variation of only one parameter in the microphysical parameterization scheme can have substantial impacts on the hurricane simulations. Therefore, in order to understand why microphysical processes affect the intensification of hurricanes, more details about the representations and effects of such processes need to be examined.

c. Impacts on Hydrometeor Distribution within Hurricane

To produce adequate QPFs for hurricanes, the effects of different processes on the horizontal and vertical distributions of hydrometeors must be quantified. Here, an analysis of how microphysical and thermodynamic processes affect these distributions is

made. The analysis of Braun and Tao (2000), who previously showed the importance of boundary layer processes for the horizontal distribution of condensate, is not repeated.

Figure 12 shows the distribution of surface reflectivity for 3 of the different microphysical schemes depicted in Fig. 7 for simulations with the Burk-Thompson boundary layer scheme. Even though the mean reflectivity, for points with $Z > 0$ dBZ, between simulations varies by only 1.7 dBZ, substantial differences in the horizontal distribution of precipitation are noted. Because minor differences in simulations could cause different temporal evolutions, it is important to not only examine how the horizontal distributions of reflectivity, hydrometeors, or rain rate vary between simulations, but also to determine how the mean values and the frequency distributions of the above quantities vary between simulations. Further, because latent heating is the energy source that maintains hurricanes, differences in hydrometeor frequency distributions can substantially affect the latent heating, and hence the time evolution of storms.

Regardless of the choice of microphysical parameterization scheme, the larger surface reflectivities from model simulations are much bigger than larger surface reflectivities observed by the P-3 radar, even though the resolution of the observations and model simulations are comparable. This suggests that the physical representations in the model are overpredicting precipitation amounts in these areas and reasons for these discrepancies need to be explored. On the other hand, the model does predict an asymmetrical distribution of precipitation in agreement with the NOAA radar observations, and the simulated size of the hurricane eye, ranging from 50 to 80 km for the different simulations, is in reasonable agreement with the observations. The exact

asymmetrical nature of the eyewall observed by Marks et al. (2003), however, is not seen. The typical widths and spacings of the rainbands, of 12 and 21 km, also compare reasonably well with the observations.

To adequately reproduce observations, not only is it necessary to consider mean and maximum reflectivity, it is also necessary to consider the distributions of reflectivity and rainrate. Figure 13 shows the area of the hurricane having rain rate above the threshold plotted on the horizontal axis varies depending on the microphysical scheme represented by different line types. The total amount of precipitation associated with the hurricane does not vary substantially between the different simulations, with the total volume of rain reaching the ground at this time varying from $7.7x10^8$ to $7.4x10^8$ to $8.9x10^8$ m^3 h^{-1} for the simple ice, mixed-phase, and Goddard microphysics schemes respectively. However, despite there being no major differences in the mean rainfall rates (varying from 4.24 to 4.35 to 5.35 mm h^{-1} for simple ice, mixed-phase and Goddard microphysics respectively) and in the standard deviations of rainfall rates (from 9.2 to 10.5 to 11.9 mm h^{-1} for the same three same cases), there are substantial differences between precipitation distributions of precipitation, especially for the higher rainfall amounts.

The differences between the simulations are significant because the area of the storm with rain rates above some of the higher thresholds (e.g., 50 mm h^{-1} and above) varies by almost up to an order of magnitude given the logarithmic scale plotted. Given that these high rain rates are most responsible for inland flooding that can cause some of the major destructive impacts of hurricanes and loss of life, these differences are significant. In general, simulations with greater frequency of higher surface rain rates

correspond to simulations with lower center pressures and larger surface winds, which seems reasonable given the greater release of latent heat that would be expected to occur.

To determine the relative importance of varying microphysical parameterization schemes, similar analysis is conducted for the other sensitivity studies. Examination of the distribution of surface reflectivity for simulations with varying boundary layer schemes showed differences between simulations, but did not conclusively show whether significantly different trends existed. However, the simulation with use of the Blackadar scheme did seem to give a hurricane with significantly smaller areas than the simulations with the Burk-Thompson or Eta boundary layer scheme. Figure 14 shows the variation of hurricane area with rain rate above a threshold as a function of rain rate for simulations with varying representations of the planetary boundary layer. Even though the minimum center pressure and maximum surface winds differed substantially for these simulations, the simulated distributions of rain rates do not. The fact that areal distributions of rain rates for different boundary layer simulations are similar helps show that there is no simple correlation between rain rate distributions and storm intensities, and that dependencies on other dynamic and thermodynamic factors must be considered.

Figure 15 shows distributions of surface reflectivity at 0000 UTC on 11 September for simulations with varying representations of graupel fall speed, all of which are within the range of plausible solutions identified by McFarquhar and Black (2003). As for simulations with varying microphysical and boundary layer schemes, there are differences in distributions that are hard to quantify from surface reflectivity distributions. For simulations with lower fall speeds, there is more time for the graupel to be advected further from the updrafts associated with its production, and hence different

horizontal distributions of precipitation might be expected to result since graupel is converted to rain by varying hydrometeor conversion processes. However, there are no clear differences in storm horizontal size in Fig. 15 depending on graupel fall speed. There may be no effect on storm horizontal size because graupel only occurs at close proximities to updrafts (e.g., AMPR data shown in Fig. 3), and hence rainbands, which are more controlled by the advection of snow, might be more affected by snow velocities than graupel velocities.

However, the representation of graupel fall speed still has an impact on the intensity of precipitation forecasts for the storm, as shown in Figure 16 that plots the area of the hurricane having rainrate above the threshold plotted on the horizontal axis. There is no simple relationship between fall speed and the occurrence of higher rain rates (e.g., faster fall speeds give more intense rain rates in general), as the simulation with fastest and slowest graupel fall speeds have less intense rain occurring than the simulation with the medium graupel fall speeds. These differences are significant given the logarithmic scale used in Fig. 16. Since there is no simple relationship between storm intensity and graupel fall speed, but differences between simulations do exist (Fig. 9), this suggests that dynamical effects associated with the release of latent heat during various microphysical conversion processes are crucial for affecting the intensification of the hurricane and for an understanding of storm dynamics.

Simulations with varying condensation schemes again show that microphysical conversion terms between hydrometeor categories do not allow determine the distribution of the condensate within the tropical cyclone. Distributions for the base case are again compared against results from the simulation with the use of the new condensation

scheme, which limits the artificial increase in Θ_e that occurs in some existing condensation schemes. Figure 17 shows the hurricane area having rainrate above the threshold plotted on the horizontal axis. Differences between simulations are highly noticeable and larger than the differences produced by the use of different microphysical schemes (Fig. 13), boundary layer schemes (Fig. 14) or graupel fall speeds (Fig. 16). The simulation with the new condensation scheme produces much lower rain rates, and this is especially noticeable by the more infrequent occurrence of the higher rain rates; this is logical, because the higher rain rates are associated with the intense rain band at the hurricane eye wall, where conventional parameterization schemes would be expected to most over predict the amount of condensation occurring, and hence, the amount of rain produced. This figure is important for showing that many other factors, in addition to varying representations of microphysics, are also responsible for the different distributions of precipitation noted in the different simulations.

d. Impacts of Variances Between Simulations

The major driving force behind a hurricane is the release of latent heat that is associated with conversions between the phases of water and varying hydrometeor categories. If simulations with varying representations of microphysical, thermodynamic, or boundary layer processes are producing different estimates of latent heating and hence feedbacks on dynamical processes that is affecting the structure and evolution of hurricanes, it should be possible to see differences in the updraft and downdraft characteristics in the model simulations. For the purpose of this study, an updraft or downdraft is defined as any grid box where the air velocity is greater than or less than 1 m s^{-1} respectively. This is similar to definitions used by Jorgensen (1985) and Houze

(1988) in that Jorgensen's definition assumed these fall speeds existed in aircraft observations for 5 consecutive seconds, which approximately corresponds to 1 km, and Houze's definition assumed the air motion had a greater magnitude than that of stratiform ice particles, which is on the order of 1 m s^{-1}.

Figure 18 shows how the updraft and downdraft characteristics vary for the different microphysical schemes, and Figure 19 shows how these characteristics vary for simulations using different graupel fall velocities. The plots are shown for a number of different altitudes located near the freezing level where latent heat release is most important. Substantial differences in the updraft and downdraft characteristics are noted between simulations showing that the microphysical processes are substantially feeding back upon storm dynamics. For example, simulations with more detailed representations of microphysics, greater number of categories in the Goddard scheme, typically have larger updrafts and downdrafts than those simulations with less detailed representations of microphysics. These were also the simulations that produced larger areas with intense rainfall rates (Fig. 13). Similarly, the base simulation produced greater updrafts and downdrafts than simulations with enhanced or reduced graupel fall velocities, the simulations that also produced larger areas of intense rain (Fig. 16). The differences between updrafts and downdrafts for the different simulations categorically proves that these conversion processes must be adequately represented in order to adequately determine the life cycle of a hurricane.

In an attempt to determine which schemes or choice of schemes might be better representing processes occurring within hurricanes, comparison of observed and simulated reflectivity is performed. The modeled reflectivity is computed from the

hydrometeor mixing ratios, assumed size distributions, and difference surface characteristics of the different hydrometeor species. Figure 20 shows a cross-section of modeled reflectivity from the base simulation and for the new iterative condensation scheme. Compared to Fig.4, the substantially larger modeled values of reflectivity compared to the observations at all levels can be clearly seen in both simulations. However, a plot of the frequency of occurrence of different values of reflectivity showed that the frequency of the highest reflectivity values were reduced with the use of the new iterative condensation scheme, in analogy to the reduction of the frequency of occurrence of higher rainrates seen in Fig. 17.

An indirect comparison of the modeled updrafts and downdrafts can also be made, using the EDOP observations shown in Figure 4. Because EDOP measures the speed of particle zones to and away from the airplane on which it is installed, the EDOP observations represent the combination of air velocity and the velocity of particle zones. For particles above the melting level, the fall speeds are approximately 1 to 3 m s^{-1}, depending on the mixture of snow, graupel, and ice, whereas for particles below the melting level, the mass-weighted fall speeds range between 5 to 10 m s^{-1}, depending on the sizes of the raindrops. These particle speeds should be considered when interpreting the Doppler velocities shown in Figure 4. A couple of differences between the observations and the simulations can be noted by comparing the updraft/downdraft statistics (e.g., Fig 18) and cross-sections of air motion (Figures not shown). First, the significant updrafts, with values up to 10 m s^{-1}, present in the base simulation are not seen in the EDOP data. This, combined with the substantial overestimate of the radar reflectivity values in the model compared to the EDOP data, suggests that none of the

microphysical parameterization schemes are adequately capturing the quantitative precipitation estimates. Note also that the downdrafts predicted by the models do not vary as much as do the updrafts between different condensation schemes, estimates of fall velocity, and depending on the condensation scheme, and given typical fall speeds of raindrops are not inconsistent with the EDOP downdrafts. Because both the updrafts, and rainrate and reflectivity values are much lower for the simulations with enhanced or reduced graupel fall speeds and for the simulations with the use of the new iterative condensation scheme, more consistent with observations, this strongly suggests that some of the basic physical representations in the model may not be adequately represented.

The over prediction of rain rate for our base simulation compared against observations may be caused by an overprediction of graupel, since graupel ultimately leads to the formation of rain. This may also cause the enhanced reflectivities seen in the upper levels in Fig. 20. Figure 21 shows histograms of graupel at multiple levels for the base simulations with the Goddard microphysical scheme. Compared against graupel mixing ratios observed in other hurricanes (e.g., Figure 10 in McFarquhar and Black 2003), the simulated graupel mixing ratios are much higher and may be causing the overprediction in rainfall amount. This cannot be categorically stated because in-situ observations of graupel mixing ratios from Hurricane Erin at these levels are not available to compare against the simulations. However, comparison with the AMPR radiometric data further suggest that the modeled values of graupel are much too high because such high amounts of graupel are not necessary to explain the observed AMPR brightness temperature.

Another test of the simulations can be made not by examining the amounts of graupel, but rather its spatial distribution and its spreading in horizontal directions compared to observations. Figure 22 shows graupel mixing ratio and updraft velocity plotted as a function of horizontal distance from the center of the hurricane for simulations with varying graupel fall speeds. Different angles of cross-section are used to examine the relationship between updraft velocity and graupel mixing ratio in Fig. 22 to ensure that an intense rain band and significant amounts of graupel are included in the cross-section. Graupel occurs over a very narrow band of 10 to 40 km, well correlated with the location of the updraft in the model simulation. This trend is true regardless of the graupel fall speed used in the simulation. Compared to the AMPR observations in Fig. 3, it would appear that the smaller band widths associated with the lower or higher graupel fall speed simulations may replicate the scattering behavior better from graupel. The most important aspect, though, is that the graupel mixing ratios seem to be over predicted by the model compared to the AMPR observations. It is also worth mentioning that McFarquhar and Black (2003) showed that the size distribution characteristics were very different in regions of the tropical cyclone with substantial updrafts or downdrafts compared to more stratiform regions. These differences could affect fall velocities and hence the feedbacks on dynamics, which may impact the hurricane simulations. Subsequent studies will examine effects due to the dependence of microphysical parameters on the updraft velocities.

d. Impacts on Inner Eye Thermodynamics

Not only do microphysical processes impact the distribution of hydrometeors, but also the representation of condensation. Figure 10 previously showed that a less intense

storm with lower surface winds was obtained with the use of a new condensation scheme that better limited an artificial increase in Θ_e. Further, the maximum rain rates and reflectivity was produced for such simulations suggesting that they better agree with observations and hence might be better representing physical processes that occur in hurricanes. Histograms examined from the simulations shown in Fig. 20 also showed that the reflectivity at all levels in the vertical is substantially less than for the base simulation compared to the iterative condensation scheme. This is definitely associated with differing dynamic effects, as the magnitudes of the updrafts and downdrafts are substantially lower for the simulation with the new condensation scheme are substantially lower than those produced with the base condensation scheme as shown in Figure 23. Simulations with varying microphysical representations failed to show a significant decrease in the amount of graupel aloft, a common problem with mesoscale simulations of hurricanes, and also failed to limit the artificially high R that are typically associated with mesoscale simulations of hurricanes. Simulations with varying graupel fall velocities improved the simulation somewhat, but not to the degree that the simulations with the new condensation scheme. Thus, the new condensation scheme might at first appear to give a better representation of the hurricane. However, an examination of inner eye thermodynamics must also be made in order to determine if these new condensation schemes are better representing the processes that occur within tropical cyclones.

Figure 24 shows an azimuthally and time-averaged cross-sections of Θe in the inner domain for the base simulation and for the simulation with the new iterative condensation scheme. A couple of differences between the cross-sections are evident, namely there is lower Θ_e near the surface associated with the use of the new iterative

condensation scheme, and lower Θ_e around 500 mbar in the dry region of the hurricane for the base simulation. Better agreement with Θ_e values computed using the dropsondes released from the ER-2 are obtained near the surface for the new iterative condensation scheme, and the overestimates of Θ_e compared to these observations as found in all other simulations are no longer present. At first, this tends to suggest that the iterative condensation scheme is doing a much better job simulating processes within the eye wall and giving a better representation of thermodynamics in the eye. However, for higher levels, this is not the case.

When vertical profiles of temperature and moisture from the new iterative condensation scheme are compared against those from the base simulation and from measurements obtained in the eye of the hurricane (Fig. 25), a different perspective is realized. With the use of the iterative condensation scheme, the substantial dry layer between 800 and 300 mbar noted with the dropsonde and with the base and other simulations is not present. Because the use of the new condensation scheme leads to less condensation in the eye wall, perhaps the extra water vapor that is not condensed mixes with the dry air in the eye, hence producing a moister eye in these simulations. Alternatively, the lower updrafts associated with the new condensation scheme are less efficient at transporting water vapor to higher levels and away from the eye, allowing more moisture to ultimately reach the eye. Thus, even though certain aspects of the simulation are improved with the use of iterative condensation, other aspects do not replicate features found in the observations. The whole mixing processes, and forces acting within the eye must be considered in the future to determine the physical processes responsible for the transport of water vapor in and around the eye of the hurricane. Thus,

even though the performance of the new condensation scheme is better than existing condensation schemes in some respects, it does not do as good of a job in predicting the inner eye thermodynamics. However, it may be that its failure in these respects may be related to failures of other mixing or parameterization schemes and further investigation is required.

In reality, a new condensation scheme that conserves Θe may have to be developed in order to limit the overprediction of condensate and the artificial increase in temperature that is seen in these simulations. This may also help better determine mixing and dynamical processes leading to better simulations.

6. Conclusions

In this paper, simulations of Hurricane Erin 2001 are conducted using the NCAR/Penn State mesoscale model MM5 in order to examine the role of different microphysical, thermodynamic, and boundary layer processes on the distribution of hydrometeors and on the structure and evolution of the tropical cyclone. Observations collected during the CAMEX4 campaign are used to help interpret the simulations in order to determine which physical processes might best represent some of the physical processes occurring within tropical cyclones. Because of the complexity of processes occurring within hurricanes, statistical comparison of results and observations are performed. The principal conclusions of this study are as follows:

1) The representation of boundary layer processes are just as important as the representation of microphysical processes in predicting the strength and intensity of hurricanes.

2) Consistent with past studies, the Burk-Thompson boundary layer scheme and the Eta boundary layer scheme seem to give the best representation of boundary layer physics when compared against observations

3) Different microphysical parameterization schemes give different strengths and intensities of hurricanes. In general, schemes with more detailed physics give lower central pressures, higher surface winds, larger rain rates, and greater reflecitivities.

4) Not only do microphysical parameterization schemes affect the hurricane simulations, but also the different microphysical parameters. In particular, simulations with varying graupel fall speed had significant effects on the distributions of precipitation, the intensity of the hurricane produced, and on the updraft and downdrafts occurring in the hurricane.

5) A new condensation scheme was developed that limits the artificial increase of Qe that has been associated with the majority of condensation schemes previously used in mesoscale models. Its use produced improved hurricane simulations in that rainrate, reflectivity, and updraft characteristics were produced compared to observations. However, the temperature and moisture profiles of the eye region did not compare as well against observations as did those using conventional parameterization schemes.

The comparisons with observations presented in this paper suggest that certain parameters or schemes may do better jobs for the representation of Hurricane Erin 2001. As noted by Zipser et al. (2003), different hurricanes can have substantially different amounts of condensate contained within them, so caution must be exercised when extrapolating these results to other hurricanes or tropical cyclones. In addition, if one parameterization scheme that artificially weakens a hurricane is used in combination with another parameterization scheme that artificially strengthens a hurricane, the final result

may look reasonable. It is really impossible to tell from a single set of simulations which processes are best represented by which parameterization schemes; instead focus needs to be placed on why different parameterizations produce different simulations. This shows that future studies must place more emphasis on the physical processes that are occurring within storms, and to produce parameterization schemes with more physical basis to more adequately represent the processes that are occurring within hurricanes. The high quality observations collected during CAMEX4 and during other field campaigns are essential for proper interpretation of the model results, and identifying deficiencies in existing model approaches.

There are no simple relations between descriptive microphysical parameters, parameterization schemes, and condensation schemes, and the strength and intensity of the hurricanes, and the distributions of hydrometeors. Therefore, it is vital that a better understanding of how the different physical processes involved with the maintenance of hurricanes. Future model simulations with finer resolutions, bin-resolved or multi-moment microphysical, and more resolved boundary layer processes should substantially aid in this interpretation.

Acknowledgments: This research was sponsored by the National Aeronautics and Space Administration Convection and Moisture Experiment (CAMEX) 4 grant number CAMEX-0000-0024. These findings do not necessarily reflect the views of the funding agency. The NOAA P-3 radar imagery were obtained from the Hurricane Research Division of NOAA. The TRMM radar data were obtained from the. The remaining data sets were obtained from the CAMEX4 archive at the Global Hydrology

Resource Center sponsored by NASA's Atmospheric Dynamics and Remote Sensing Program. One of us (GM) is grateful for discussions with Scott Braun and Da-Lin Zhang that helped set the focus for this study.

Appendix

Bryan and Fritsch (2000) documented unphysically high values of Θ_e in their simulations of cumulonimbus clouds using MM5, noting that these problems existed regardless of the microphysics or boundary layer scheme used. A major reason for the high values of Θ_e calculated was that the one-step condensation equation used tended to overestimate the final value of mixing ratio and temperature, especially in the presence of vigorous updrafts. It is unknown what effects this problem may have had on past hurricane simulations, but it may be partially responsible for the higher simulated precipitation rates than found in observations. A new iterative condensation scheme is derived here to more accurately predict the modeled condensation rate.

In version 3.5 of MM5, temperature and vapor pressure are stepped forward at each time without condensation occurring, then an adjustment step is made converting excess vapor to liquid water so that the air is saturated. Following Grell et al. (1995), (q_i, T_i) represent the temperature and vapor pressure before the adjustment step. If q_i is greater than q_{si}, the saturated vapor pressure at T_i, condensation will occur so that (q_f, T_f) represent the vapor pressure and temperature after condensation and represent saturated conditions, with $q_f < q_i$ and $T_f > T_i$. The points (q_{si}, T_i) and (q_f, T_f) are connected by the Clausis-Clapeyron equation, given by

$$\frac{dq_s}{dT} = \frac{q_f - q_{si}}{T_f - T_i} = \frac{q_s L_v}{R_v T^2} \qquad \text{(A1)}$$

where R_v is the gas constant and L_v the latent heat of vaporization. The slope of the line between points (q_i, T_i) and (q_f, T_f) is determined from moist static energy conservation,

$$L_v dq = L_v(q_f - q_i) = -c_P dT = -c_P(T_f - T_i) \quad \text{(A2)}$$

In the scheme implemented in MM5, the temperature in Eq. (A1) is assumed to be T_i, and can lead to a substantial overestimate of the amount of condensation occurring within a time step. For example, assuming an increase of 0.1°C at a temperature of 20°C, the condensation rate would be overestimated by 0.25% by Eq. (A2). Although this may not seem significant, when integrated over an entire hurricane simulation this systematic error might be problematic. Further, given that air masses may rise a couple hundred meters in a given time step, the 0.1°C increase per time step is likely an underestimate.

Although it may be advantageous to develop a condensation scheme that uses Θ_e as an advective variable, the importance of overestimating condensation can be simply made through the development of an iterative condensation scheme. The temperature used in Eq. (A1) is assumed to be the average of T_f and T_i to make a more accurate estimate of condensation, the final temperature, and water vapor content. This is an iterative calculation because q_f and T_f must be recomputed a few times until the solution converges. Because the solution rapidly converges, minimal extra computational expense is required.

References:

Braun, S.A., and W.-K. Tao, 2000: Sensitivity of high-resolution simulations of Hurricane Bob (1991) to planetary boundary layer parameterizations. *Mon. Wea. Rev.*, **128**, 3941-3961.

Bryan, G.H., and J.M. Fritcsh, 2000: Unphysical thermodynamic structures in explicitly simulated thunderstorms. 10th Annual Penn State/NCAR MM5 User's Workshop, Available from http://www.mmm.ucar.edu/mm5/mm5-home.html.

Burk, S.D., and W.T. Thompson, 1989: A vertically nested regional numerical prediction model with second-order closure physics. *Mon. Wea. Rev.*, **117**, 2305-2324.

Dudhia, J., 1989: Numerical study of convection observed during the winter monsoon experiment using a mesoscale two-dimensional model. *J. Atmos. Sci.*, **46**, 3077-3107.

Fritsch, J.M., and 16 others, 1998: Quantitative precipitation forecasting: report of the eight prospectus development team, U.S. weather research program. *Bull. Amer. Meteor. Soc.*, **79**, 285-299.

Grell, G.A., J. Dudhia, and D.R. Stauffer, 1995: A description of the fifth-generation Penn State/NCAR mesoscale model (MM5). NCAR Technical Note, NCAR/TN-398+STR, 117 pp.

Halverson, J et al., 2003: Thermodynamic structure of eye of hurricane Erin. *J. Atmos. Sci.*, submitted to CAMEX4 special issue

Heymsfield, G. M., S. Bidwell, I. J. Caylor, S. Ameen, S. Nicholson, W. Boncyk, L. Miller, D. Vandemark, P. E. Racette, and L. R. Dod, 1996: The EDOP radar

system on the high-altitude NASA ER-2 aircraft. *J. Atmos. Ocean. Tech.*, **13**, 795-809.

Hong, S.-Y., and H.-L. Pan, 1996: Nonlocal boundary layer vertical diffusion in a medium-range forecast model. *Mon. Wea. Rev.*, **124**, 2322-2339.

Janjic, Z.I., 1994: The step-mountain Eta coordinate model: Further development of the convection, viscous sublayer, and turbulent closure schemes. *Mon. Wea. Rev.*, **122**, 927-945.

Karyampudi, V.M., G.S. Lai, and J. Manobianco, 1998: Impact of initial conditions, rainfall assimilation, and cumulus parameterization on simulations of Hurricane Florence (1988). *Mon. Wea. Rev.*, **126**, 3077-3101.

Krishnamurti, T.N., W. Han, B. Jha, and H.S. Bedi, 1998: Numerical prediction of Hurricane Opal. *Mon. Wea. Rev.*, **126**, 1347-1363.

Lin, Y.-L., R.D. Farley, and H.D. Orville, 1983: Bulk parameterization of the snow field in a cloud model. *J. Climate Appl. Meteor.*, **22**, 1065-1092.

Liu, Y., D.-L. Zhang, and M.K. Yau, 1997: A multiscale numerical study of Hurricane Andrew (1992). Part I: Explicit simulation and verification. *Mon. Wea. Rev.*, **125**, 3073-3093.

Liu, Y., D.-L. Zhang, and M.K. Yau, 1999: A multiscale numerical study of Hurricane Andrew (1992). Part II: kinematics and inner-core structures. *Mon. Wea. Rev.*, **127**, 2597-2620.

Lord, S.J., and J.M. Lord, 1988: Vertical velocity structure in an axisymmetric, nonhydrostatic tropical cyclone model. *J. Atmos. Sci.*, **45**, 1453-1461.

Lord, S.J., H.E. Willoughby, and J.M. Piotrowicz, 1984: Role of a parameterized ice-phase microphysics in an axisymmetric, nonhydrostatic tropical cyclone model. *J. Atmos. Sci.*, **41**, 2836-2848.

Marks, F.D., 1985: Evolution and structure of precipitation in Hurricane Allen (1980). *Mon. Wea. Rev.*, **113**, 909-930.

Marks, F.D., S. Aberson, and J. Dunion. 2003:

McCumber, M., W.-K. Tao, J. Simpson, R. Penc, and S.-T. Soong, 1991: Comparison of ice-phase microphysical parameterization schemes using numerical simulations of tropical convection. *J. Appl. Meteor.*, **30**, 985-1004.

McFarquhar, G.M., and R.A. Black, 2003: Observations of particle size and phase in tropical cyclones: implications for mesoscale modeling of microphysical processes. *J. Atmos. Sci.*, submitted.

Orr, B.W., and R.A. Kropfli, 1999: A method for estimating particle fall velocities from vertically pointing Doppler radar. *J. Atmos. Ocean. Tech.*, **16**, 29-37.

Pasch, R.J., and D.P. Brown, 2002: Tropical cyclone report: Hurricane Erin: Hurricane Erin, 1-15 September 2001, *Nat. Hurr. Center Report*, Available from http://www.nhc.noaa.gov/2001erin.html

Reisner, J., R.M. Rasmussen, and R.T. Bruintjes, 1998: Explicit forecasting of supercooled liquid water in winter storms using the MM5 mesoscale model. *Quart. J. Roy. Meteor. Soc.*, **124**, 1071-1107.

Rogers, R., R. Black, and M. Black, 2003: Evaluating microphysical parameterization schemes for use in hurricane environments. *J. Atmos. Sci.*, CAMEX4 special issue, submitted.

Rutledge, S.A., and P.V. Hobbs, 1983: The mesoscale and microscale structure and organization of clouds and precipitation in midlatitude cyclones. VIII: A model for the ``seeder-feeder" process in warm-frontal rainbands. *J. Atmos. Sci.*, **40**, 1185-1206.

Schultz, P., 1995: An explicit cloud physics parameterization for operational numerical weather prediction. *Mon. Wea. Rev.* **123**, 3331-3343.

Smith, E.A., X. Xiang, A. Mugnai, R.E. Hood, and R.W. Spencer, 1994: Behavior of an inversion-based precipitation retrieval algorithm with high resolution AMPR measurements including a low-frequency 10.7 GHz channel. *J. Atmos. Ocean. Tech.*, **11**, 858-873.

Spencer, R.W., W.S. Olson, W. Rongzhang, D.W. Martin, J.A. Weinman, and D.A. Santek, 1983: Heavy thunderstorms observed over land with the *Nimbus-7* Scanning Multichannel Microwave Radiometer. *J. Climate Appl. Meteor.*, **22**, 1041-1046.

Spencer, R.W., R.E. Hood, F.J. LaFontaine, E.A. Smith, R. Platt, J. Galliano, V.L. Griffin, and E. Lobl, 1994: High-resolution imaging of rain systems with the advanced microwave precipitation radiometer. *J. Atmos. Ocean. Tech.*, **11**, 849-857.

Tao, W.-K., and J. Simpson, 1993: Goddard Cumulus Ensemble Model. Part I: Model description. *Terrestrial, Atmospheric, and Oceanic Sciences*, **4**, 35-72.

Willoughby, H.E., 1998: Tropical cyclone eye thermodynamics. *Mon. Wea. Rev.*, **126**, 3053-3067.

Willoughby, H.E., H.-L. Jin, S.J. Lord, and J.M. Piotrowicz, 1984: Hurricane structure and evolution as simulated by an axisymmetric, nonhydrostatic numerical model. *J. Atmos. Sci.*, **41**, 1169-1186.

Table 1:

Series	*Simulations Performed*	*Other Conditions*
Microphysical Parameterization Scheme	Goddard microphysics Reisner mixed-phase Reisner graupel Simple Ice	35 σ levels 2 km horizontal resolution No convective scheme for D4 Betts-Miller scheme for D1 through D3 Burk-Thompson scheme and Eta scheme
Boundary Layer Parameterization Scheme	Blackadar Eta Burk-Thompson	35 σ levels 2 km horizontal resolution No convective scheme Goddard microphysics
Graupel Fall Speed Representation	(a_g,b_g) = (351.2 $cm^{.63}$ s^{-1}, .37) base (199.9 $cm^{.75}$ s^{-1}, .25) (700.1 $cm^{.25}$ s^{-1}, .75)	35 σ levels 2 km horizontal resolution Goddard microphysics Blackadar PBL scheme No convective scheme
Thermodynamic Scheme	Usual condensation Scheme New Condensation Scheme	35 σ levels 2 km horizontal resolution Goddard microphysics Blackadar PBL scheme; no convective scheme

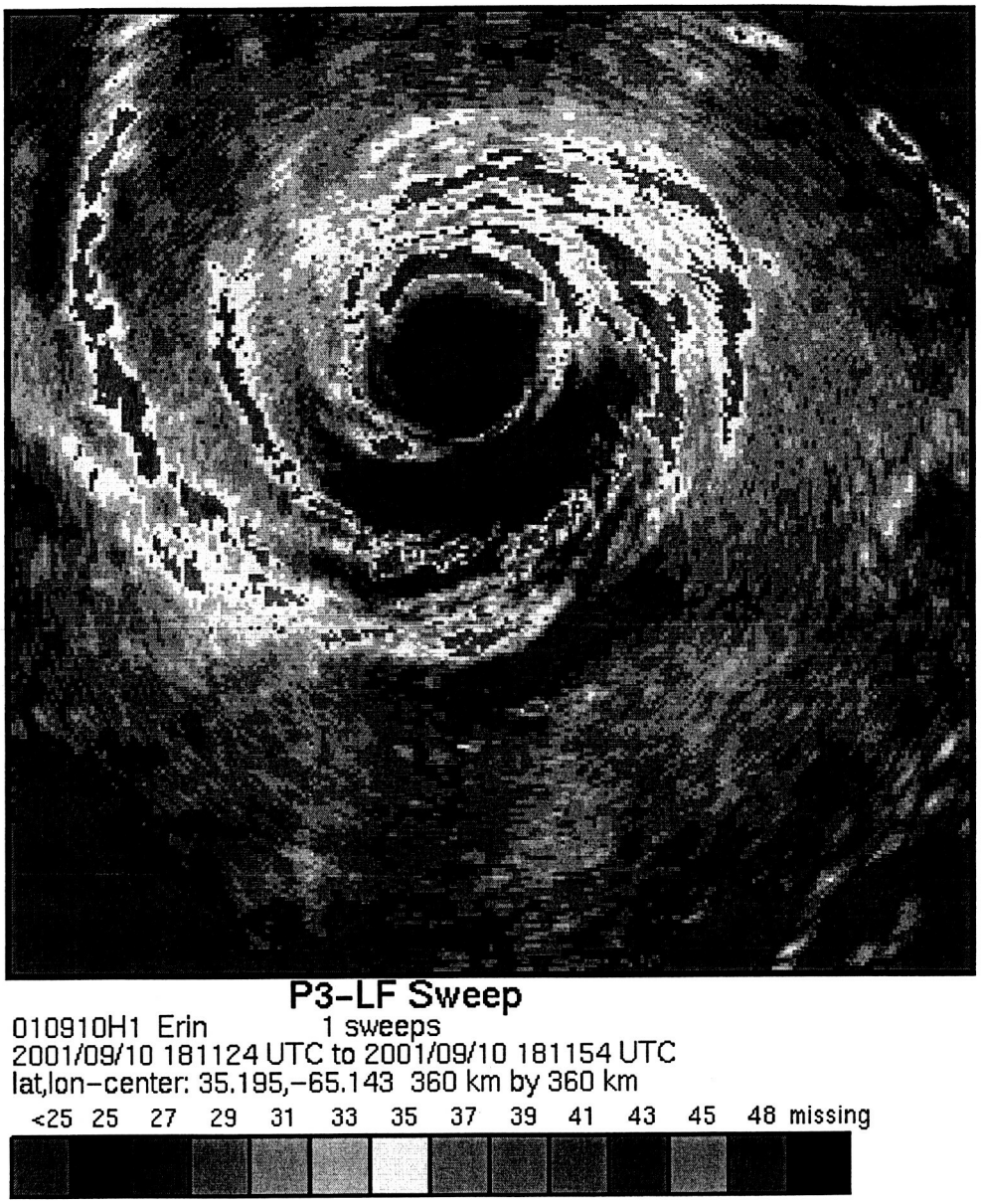

Figure 1: Radar reflectivity obtained from lower fuselage radar on board NOAA P-3 aircraft during first penetration through hurricane Erin. The picture box represents a 360 km by 360 km area, and the box is centered at 35.195°N, 65.143°W. The sweeps were made starting at a time of 181154 UTC.

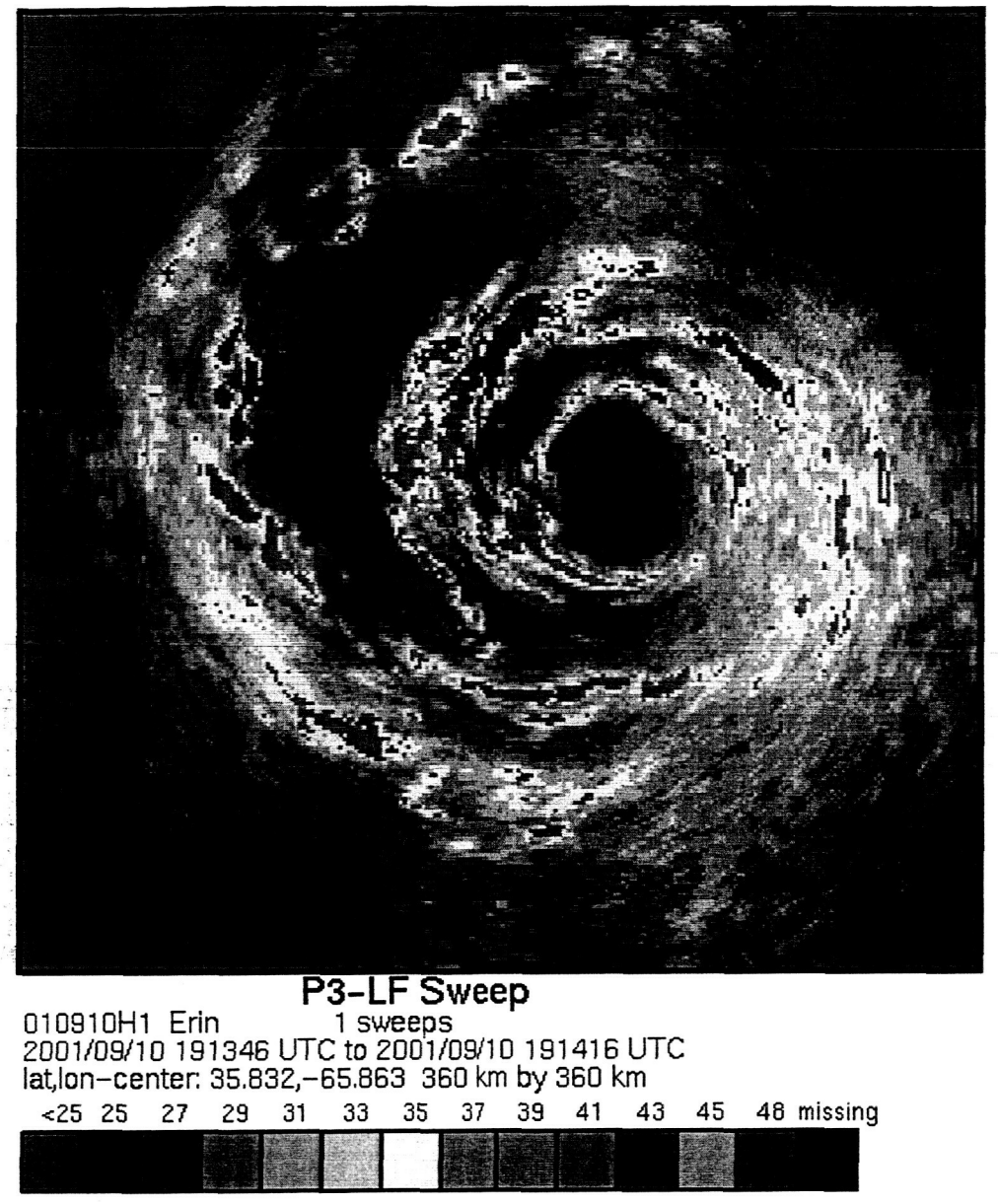

Figure 2: As in Fig. 1, except the reflectivity was made during second penetration of NOAA P-3 into hurricane Erin. Here, the box is centered at 35.832°N and 65.863°W. The sweeps were made starting at a time of 191416 UTC.

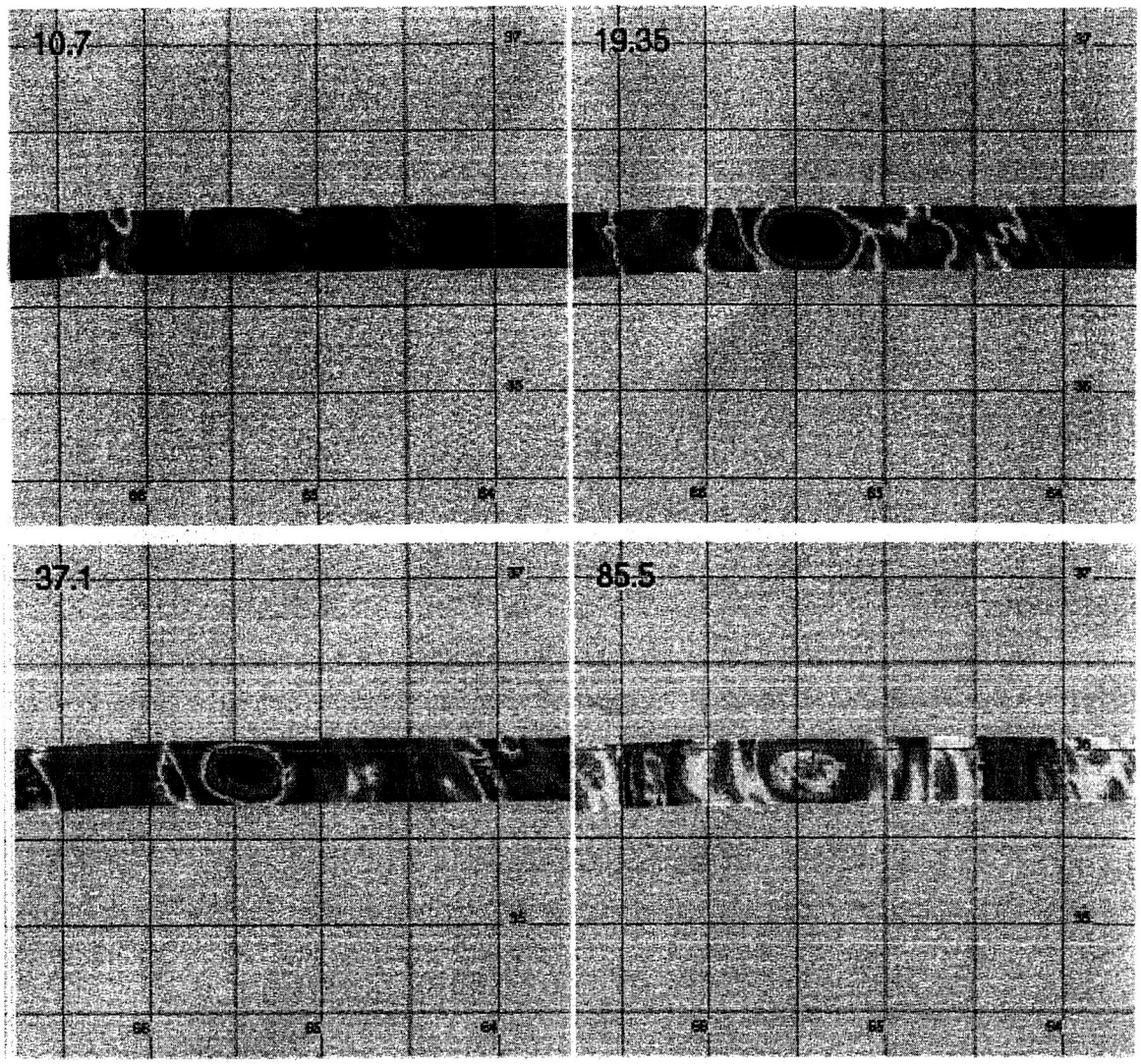

Figure 3: Brightness temperature (T_b) measured by AMPR at 10.7, 19.35, 37.1, and 85.5 GHz for transect that the NASA ER-2 flew over the eye of Erin flown between 191946 and 193459 UTC.

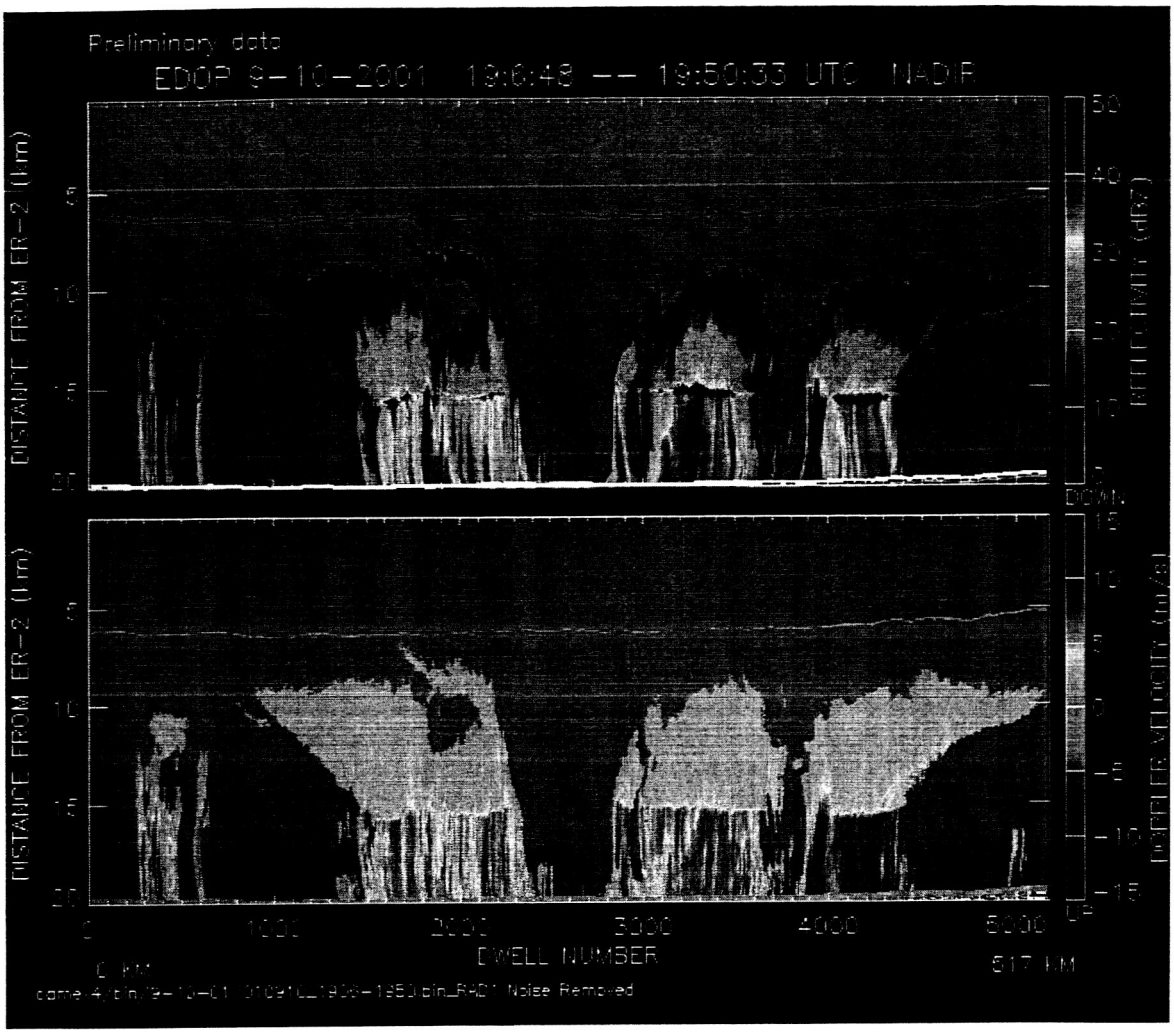

Figure 4: Reflectivity Z and Doppler velocity, a combination of ambient velocity and particle fall speed, obtained by EDOP for transect, flown to the west, shown in Fig. 2. Each dwell number corresponds to 0.5 s, so that horizontal axis is approximately 517 km. Points to right of eyewall (at 2400 to 2800 dwell number) are on the west side of the eyewall.

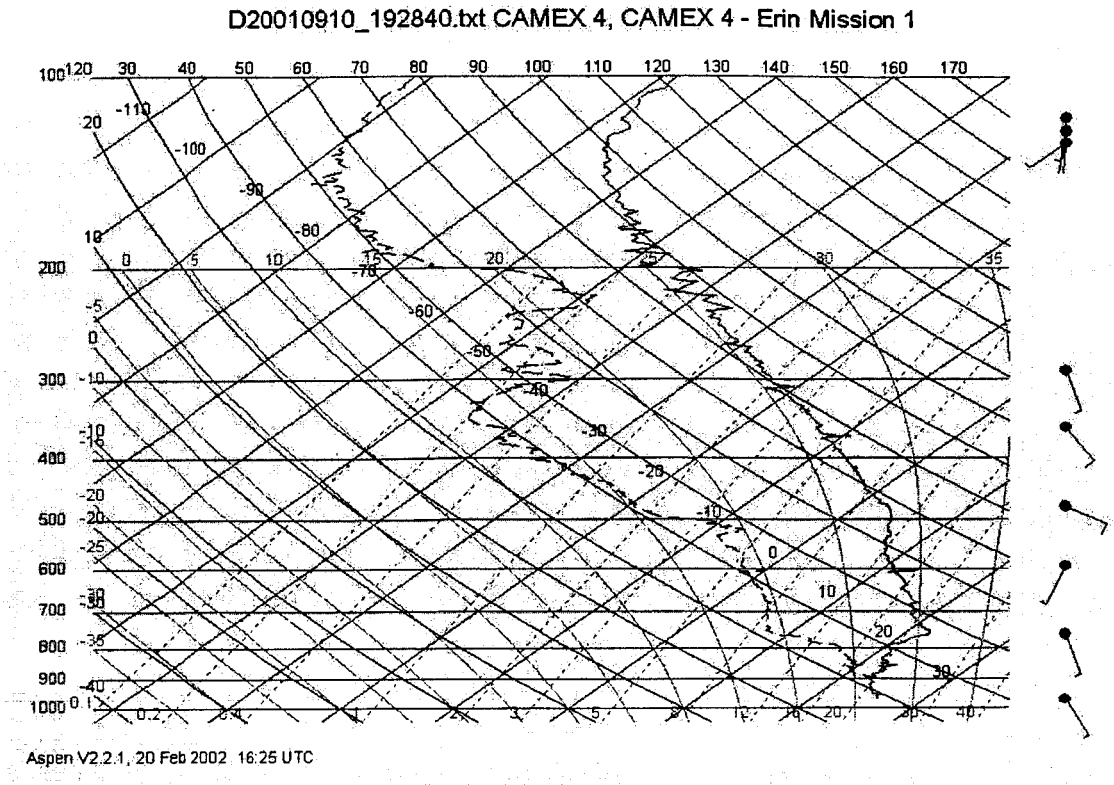

Figure 5: Vertical profile of temperature and water vapor as measured by dropsonde released from NASA ER-2 over the eye of Hurricane Erin at 192840. Red line depicts temperature profile, blue line depicts water vapor profile (**redo this figure in black and white**).

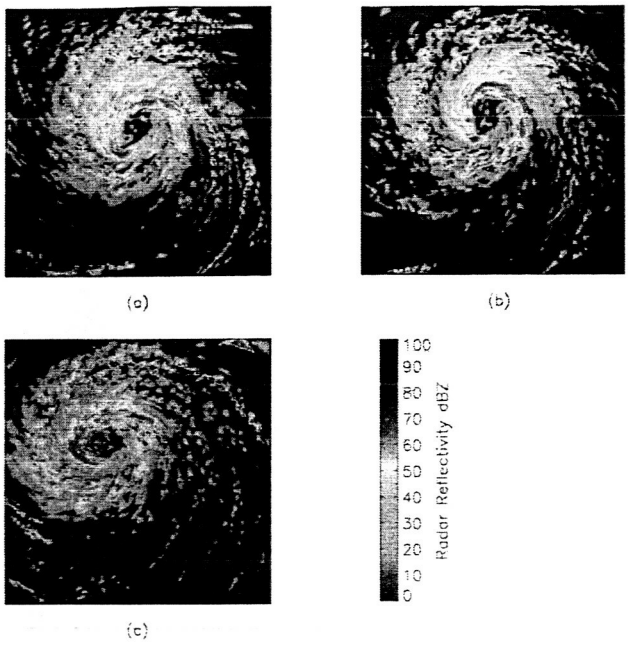

Figure 12: Horizontal distribution of surface reflectivity, dBZ, in inner domain at 0000Z on 11 September 2001 for simulations using various microphysical parameterization schemes: a) simple ice; b) Reisner et al. mixed-phase (no graupel); c) Goddard microphysics.

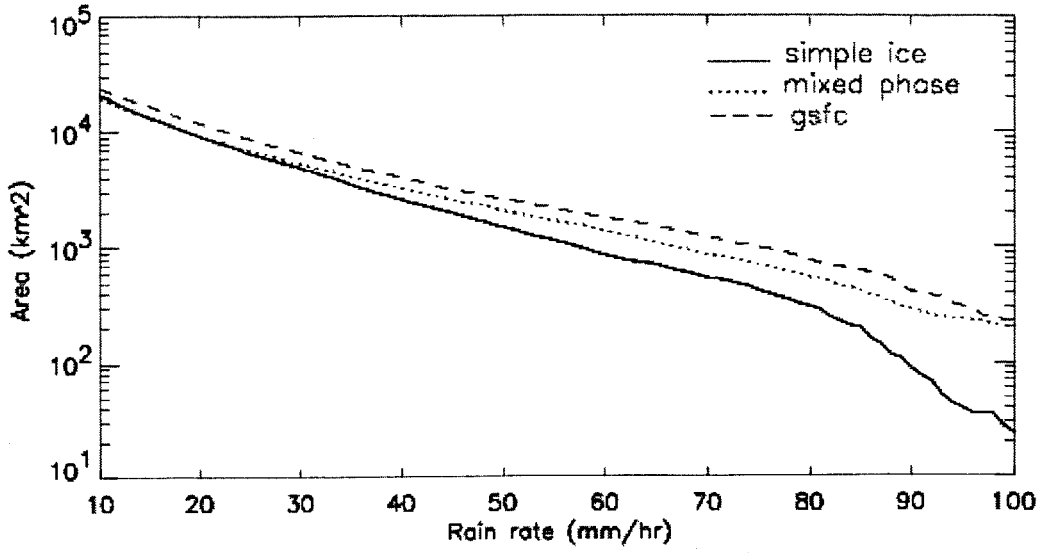

Figure 13: Area of simulated hurricane, in km^2, having rainrate above threshold plotted on the horizontal axis. Different line types represent different microphysical parameterization schemes as indicated in legend.

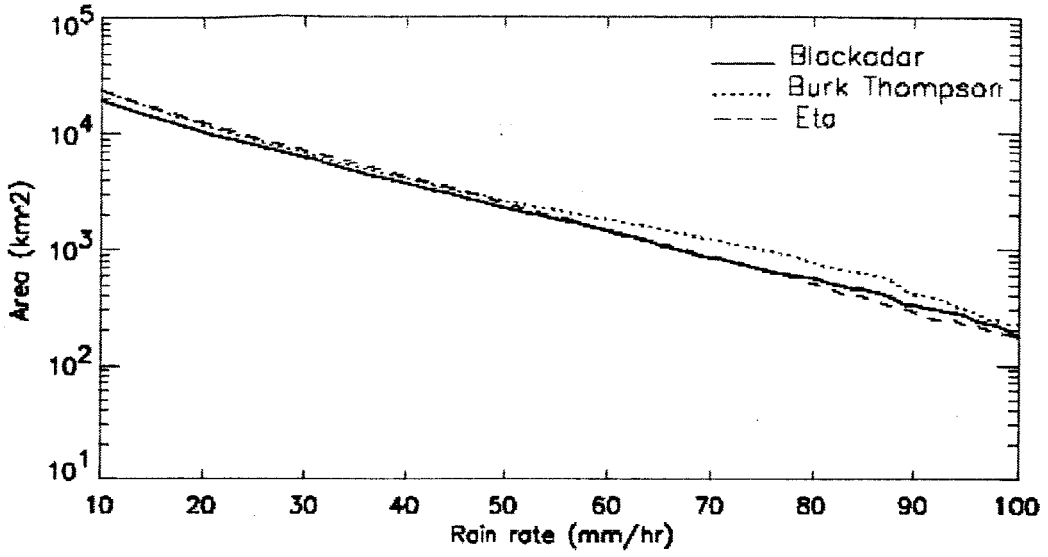

Figure 14: As in Fig. 13, except different line types correspond to simulations using different boundary layer schemes as indicated in legend.

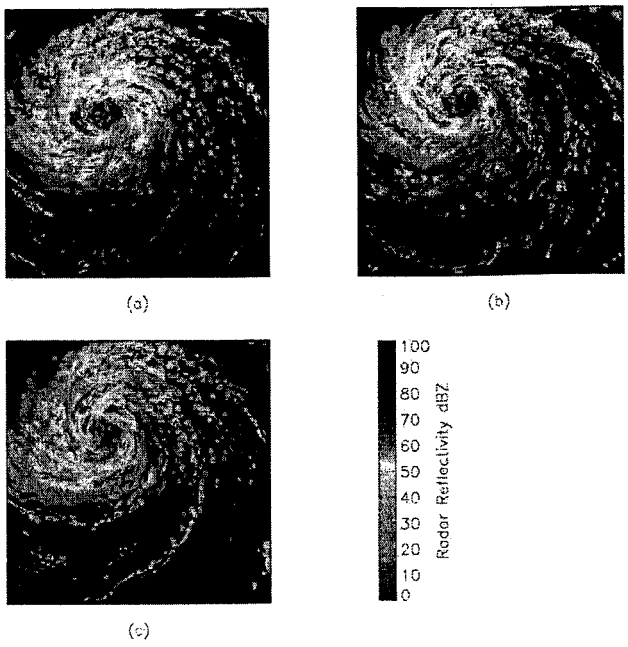

Figure 15: As in Fig. 12, except different plots correspond to simulations performed with varying representations of graupel fall speeds: (a) base conditions, (b) slower falling graupel, (c) faster falling graupel.

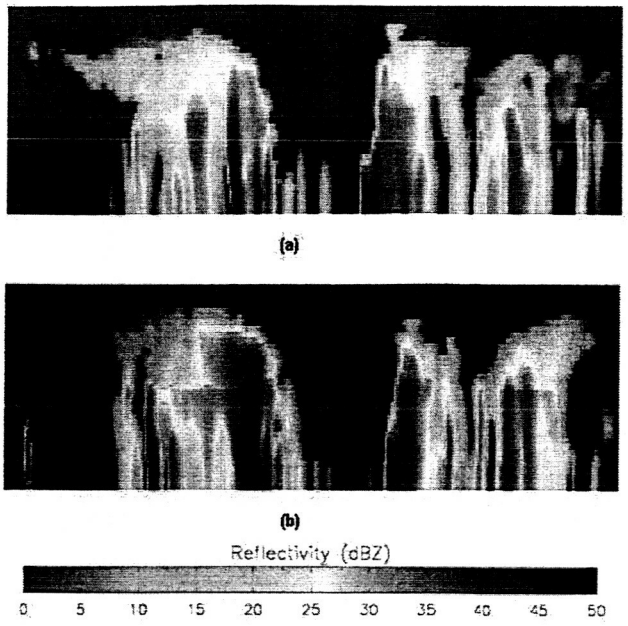

Figure 20: Cross-section of reflectivity estimated from model simulations for (a) base condition and (b) for simulation with new iterative condensation scheme at 2100 UTC on 10 September 2001. Comparison with reflectivities measured by EDOP at similar times shows that model is overestimating the reflectivity values.

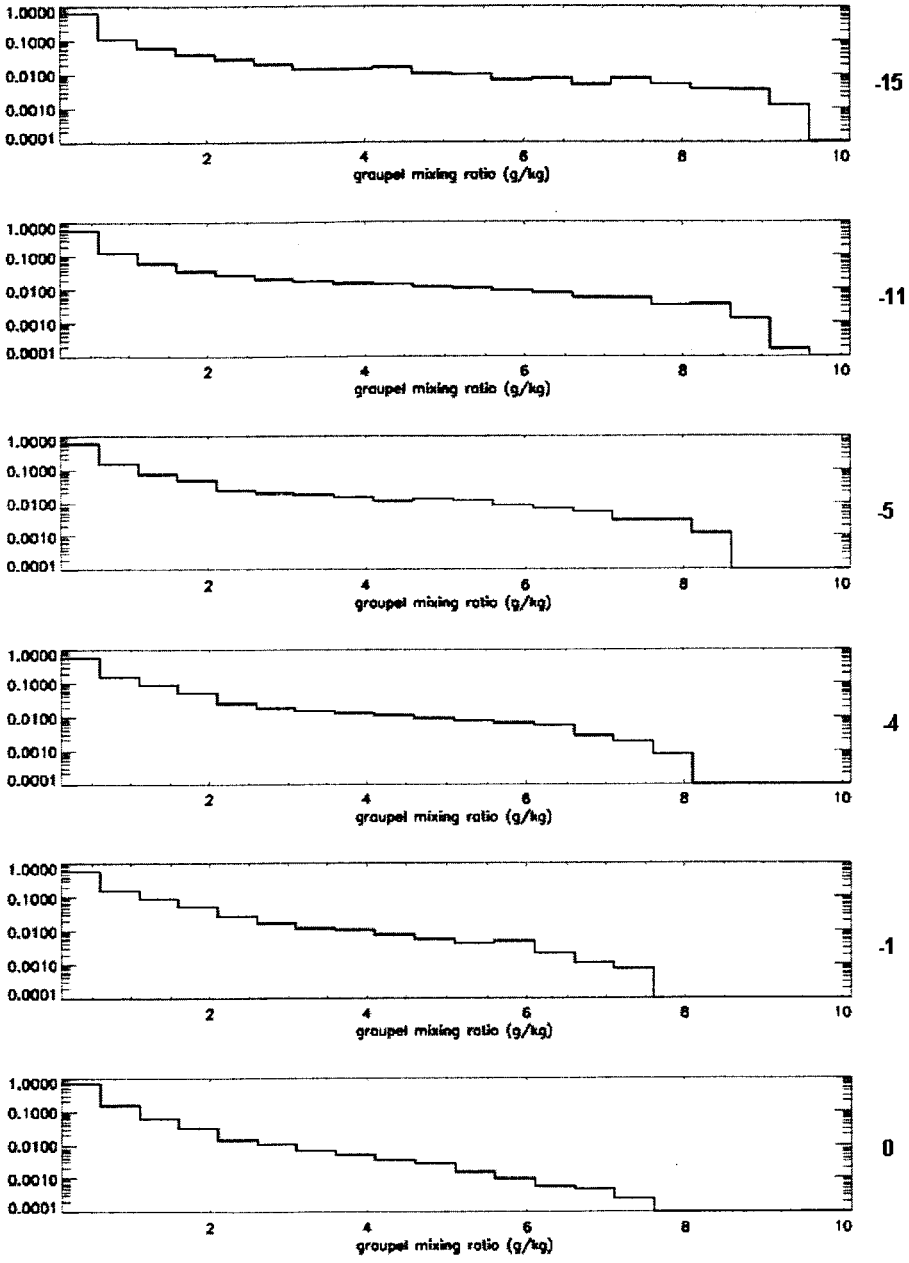

Figure 21: Histograms of graupel mixing ratios for simulations with varying graupel fall speeds.

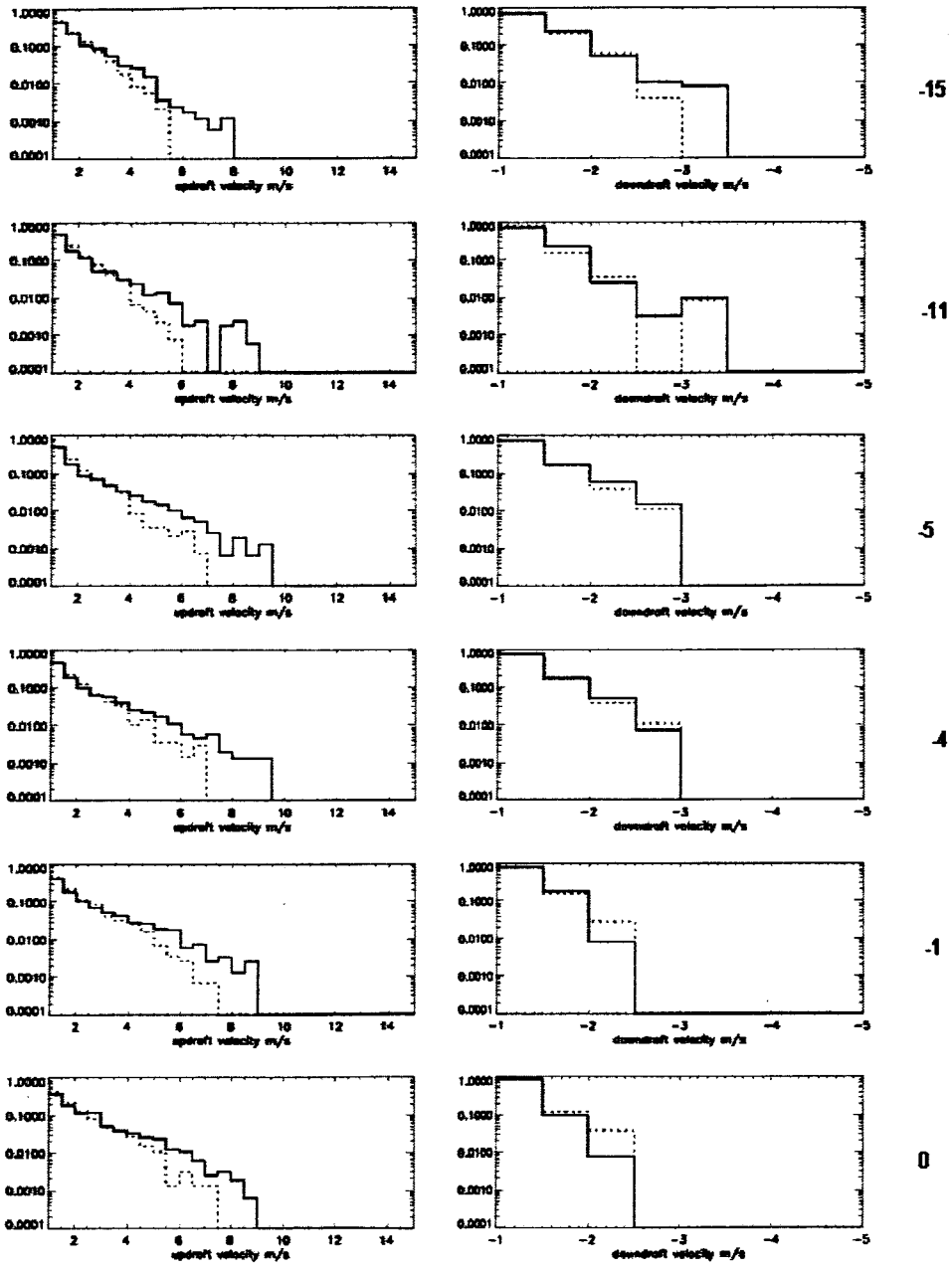

Figure 23: As in Fig. 18, except solid line represents base parameterization scheme and dashed line represents simulations with new iterative condensation scheme.

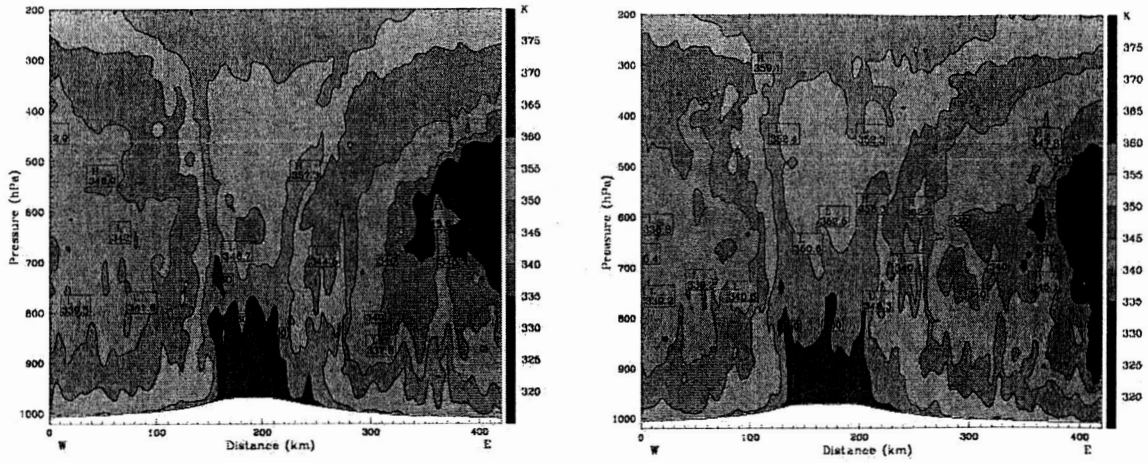

Figure 24: Cross-section of Θ_e (a) for simulation of base conditions and (b) for simulation with new iterative condensation scheme. Substantially lower Θ_e and better agreement with Θ_e from dropsonde measurements is obtained than for using base simulations.

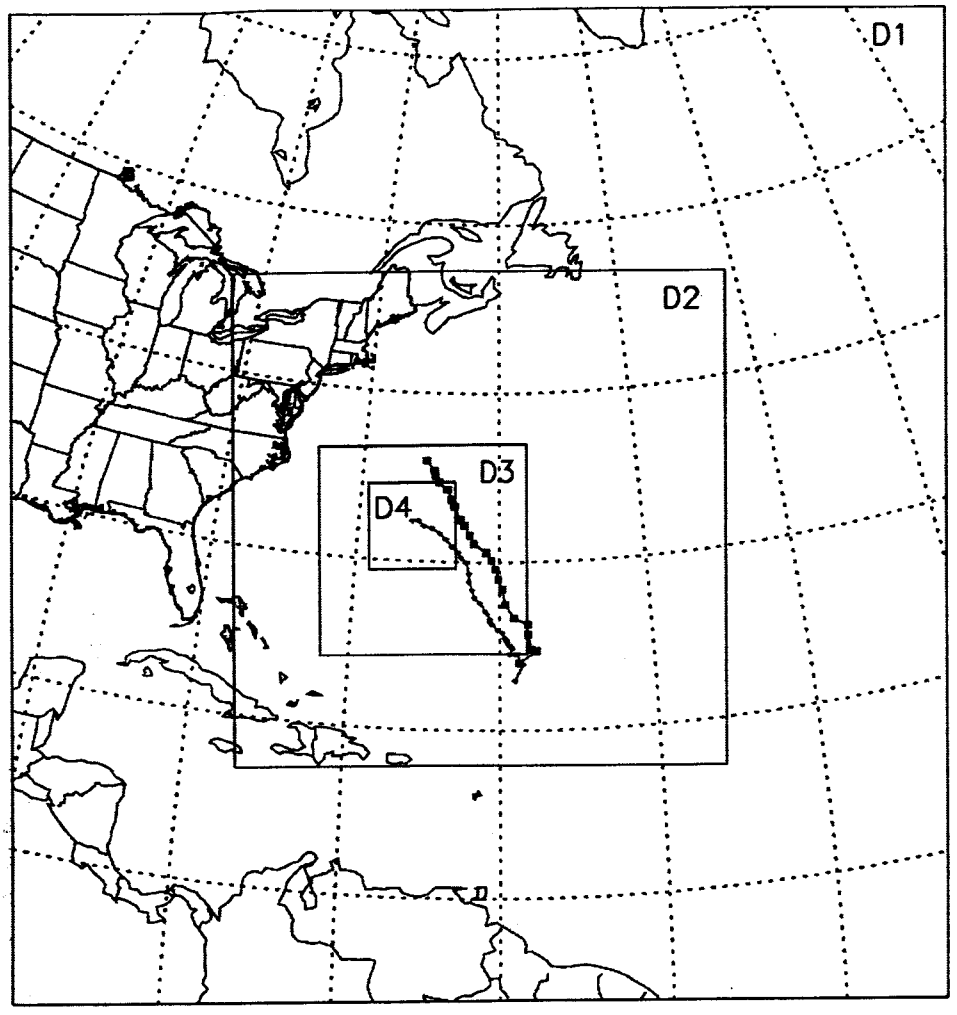

Figure 6: Domain used in MM5 base simulations of Hurricane Erin. Outer grid has horizontal resolution of 54 km, inner grids have resolutions of 18, 6, and 2 km respectively. All domains have 2-way nesting except the course domain.

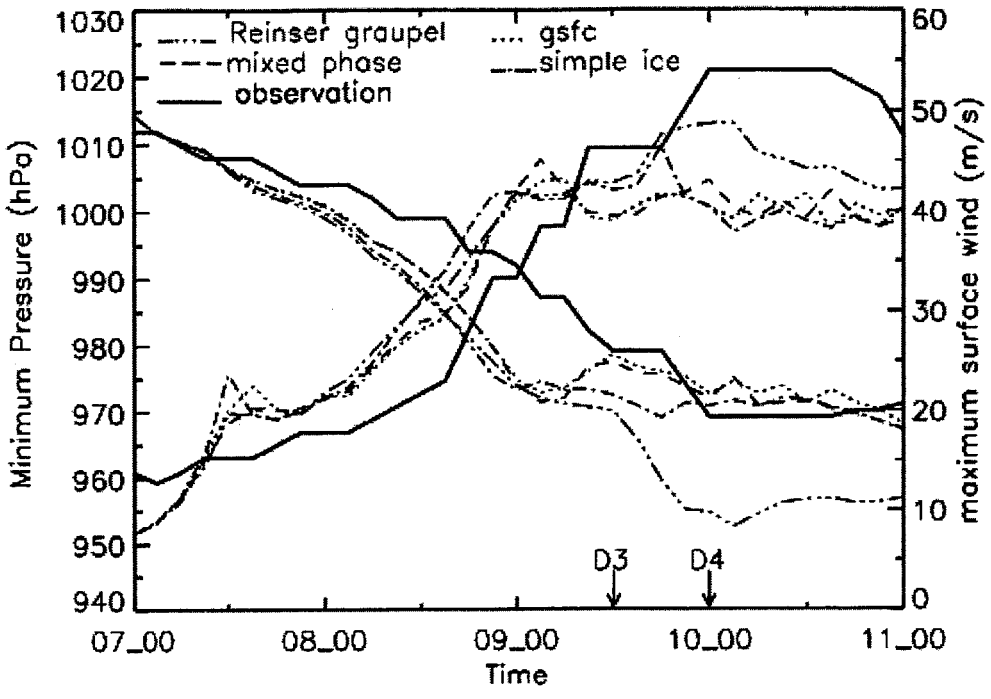

Figure 7: Temporal evolution of minimum sea-level pressure and maximum surface wind speed between 0000 UTC on 7 September 2001 and 0000 UTC on 11 September 2001. Solid lines represent observations, different line types correspond to simulations conducted with varying microphysical parameterization schemes as indicated in legend; all simulations use Burk-Thompson boundary layer scheme. D3 and D4 indicate the time at which the 6 km grid and the 2 km grid are activated respectively. See Appendix for description of other base simulation conditions.

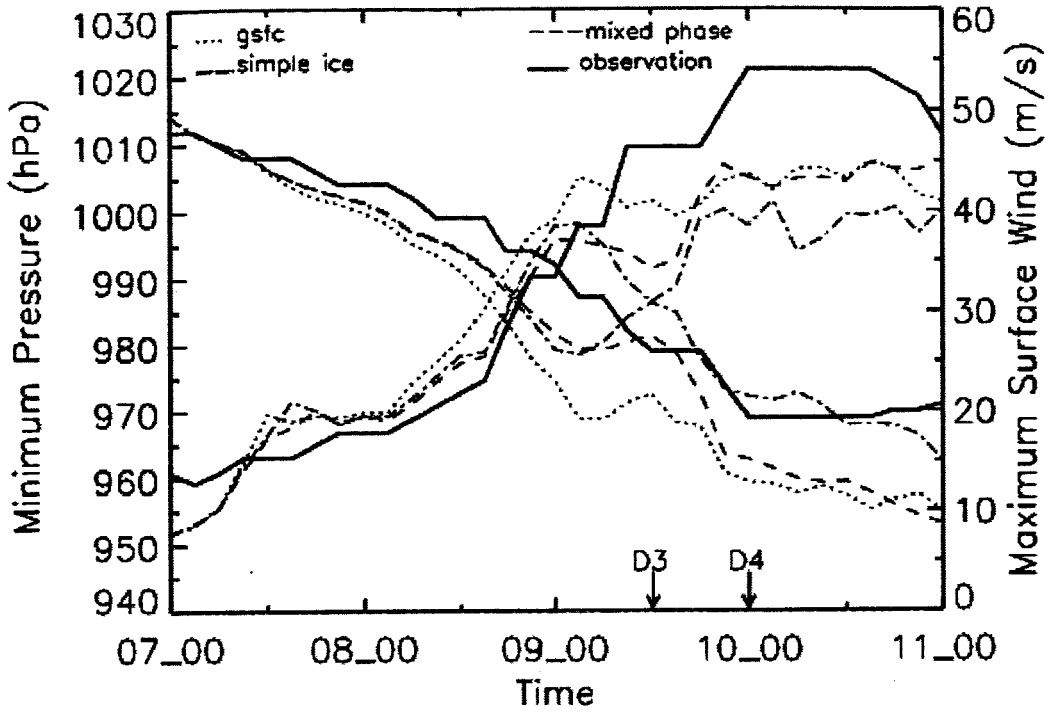

Figure 8: As in Fig. 7, except that the different microphysical simulations were all conducted using the Eta boundary layer scheme. The Reisner graupel scheme is not included in the plot because an instability in the model prevented a solution being obtained. See Table 1 for description of other base simulation conditions.

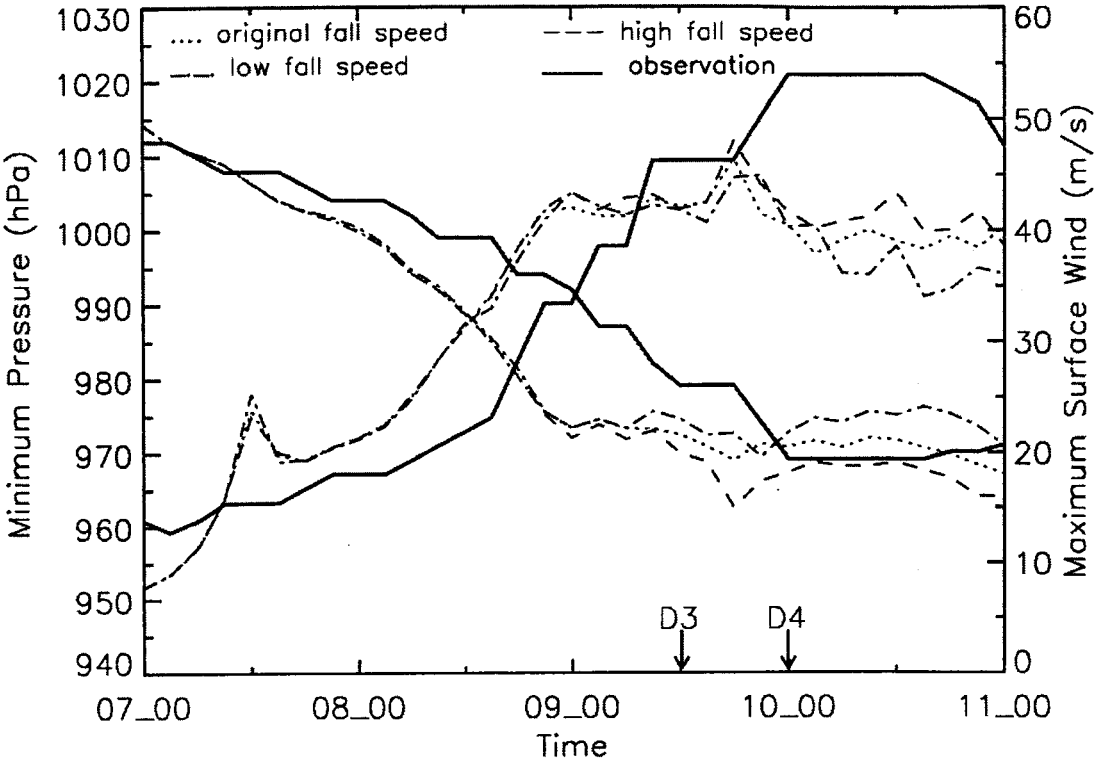

Figure 9: As in Fig. 7, except different thin lines correspond to different choice of (a_g, b_g) coefficients which describe the fall velocity of individual graupel particles. The coefficients corresponding to different fall velocities are: fast-(700.1 $cm^{.75}$ s^{-1}, .37); medium-(351.2 $cm^{.63}$ s^{-1}, .37); and slow (199.9 $cm^{.75}$ s^{-1}, .25). See Table 1 for description of other base simulation conditions.

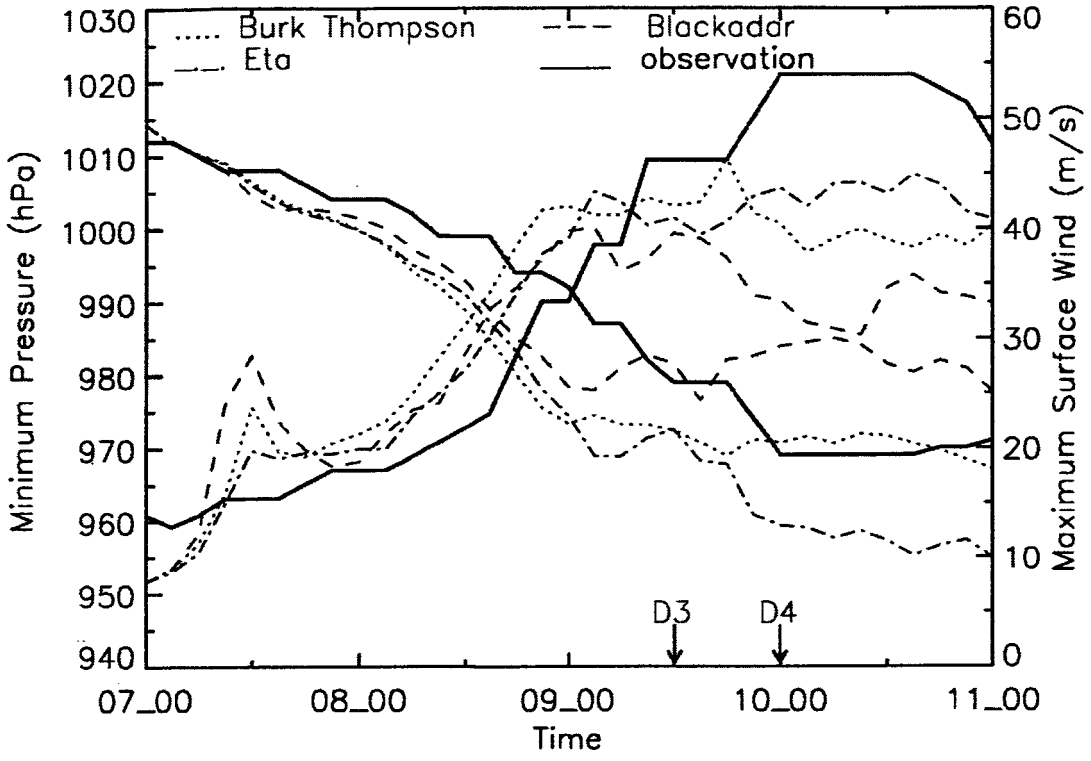

Figure 10: As in Fig. 7, except different line types correspond to simulations with different boundary layer parameterization schemes as indicated in the legend. See Table 1 for description of other base simulation conditions.

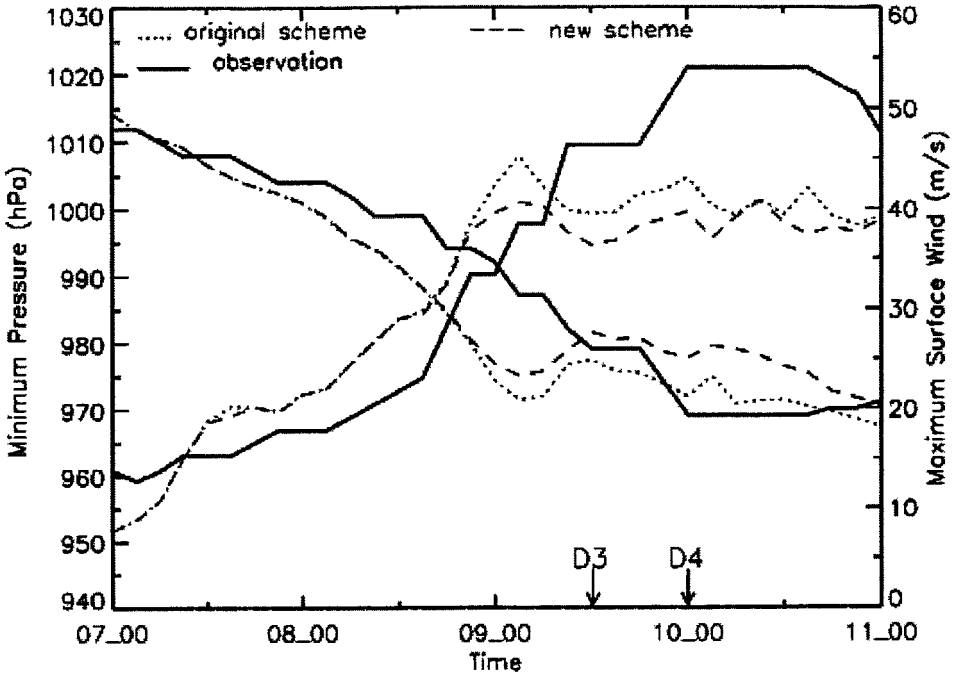

Figure 11: As in Fig. 7, except different line types correspond to use of existing condensation scheme or new iterative condensation scheme described in legend. See Table 1 for description of other base simulation conditions.

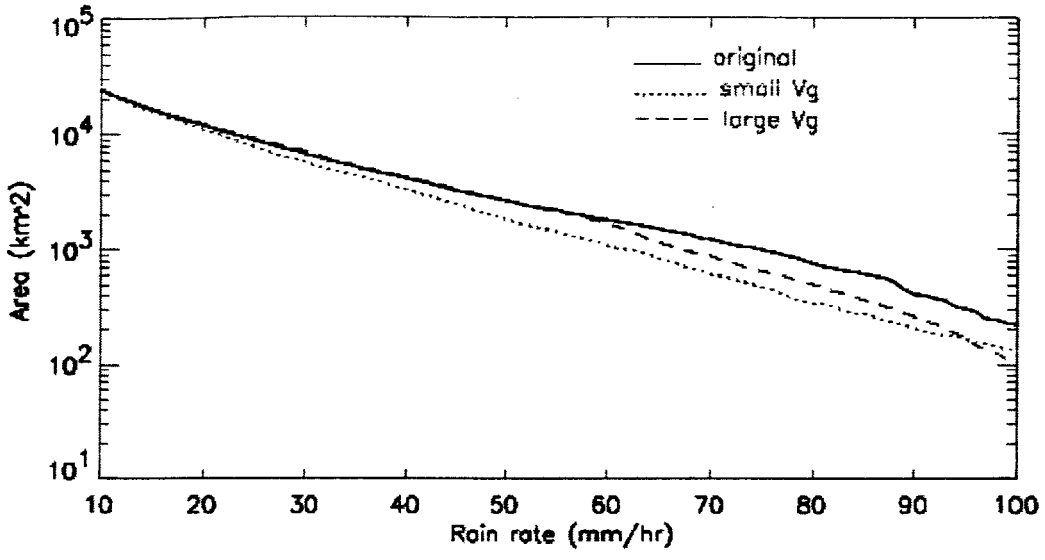

Figure 16: As in Fig. 13, except different line types correspond to simulations with varying representations of graupel fall speed as indicated in legend.

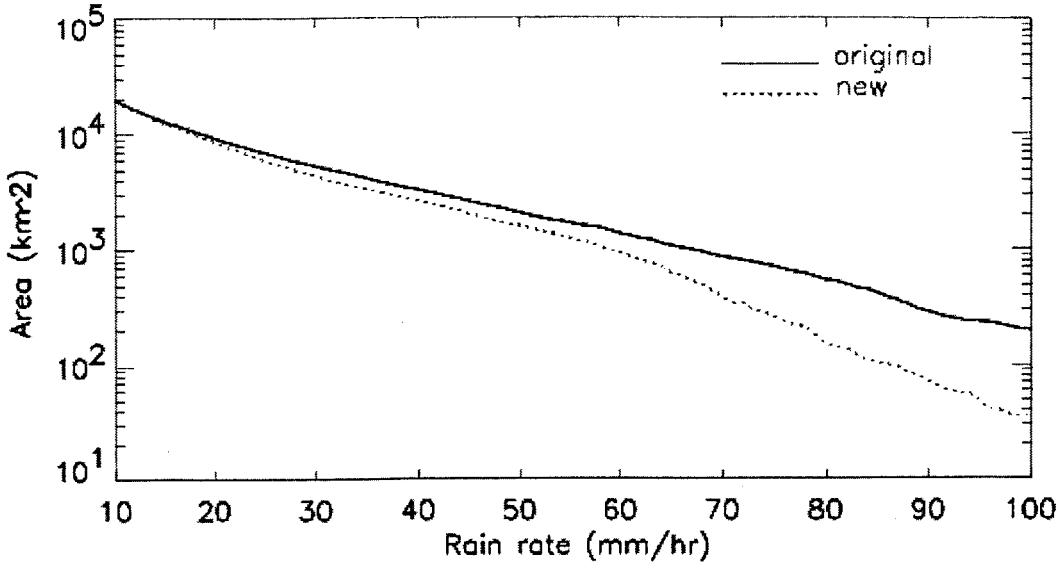

Figure 17: As in Fig. 13, except different line types correspond to base simulation and simulation with use of new iterative condensation scheme.

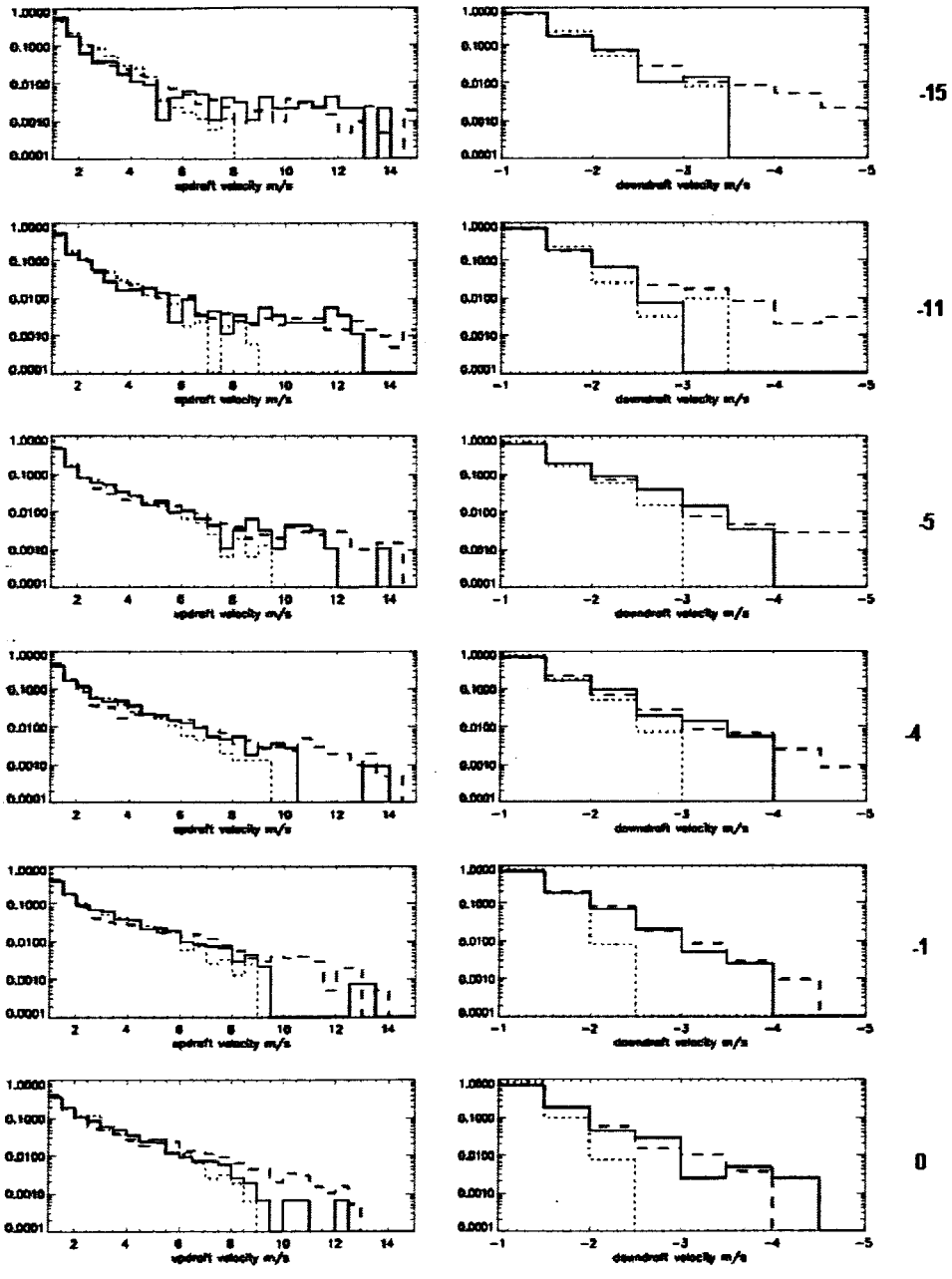

Figure 18: Histograms of frequency of occurrence of vertical updrafts and downdrafts having magnitude above 1 m s^{-1} for simulations with varying microphysical parameterization schemes: solid, simple ice scheme, dashed, Goddard scheme, dotted, Reisner mixed phase scheme. Different panels represent distributions at different σ levels, corresponding to temperatures labeled on right hand side.

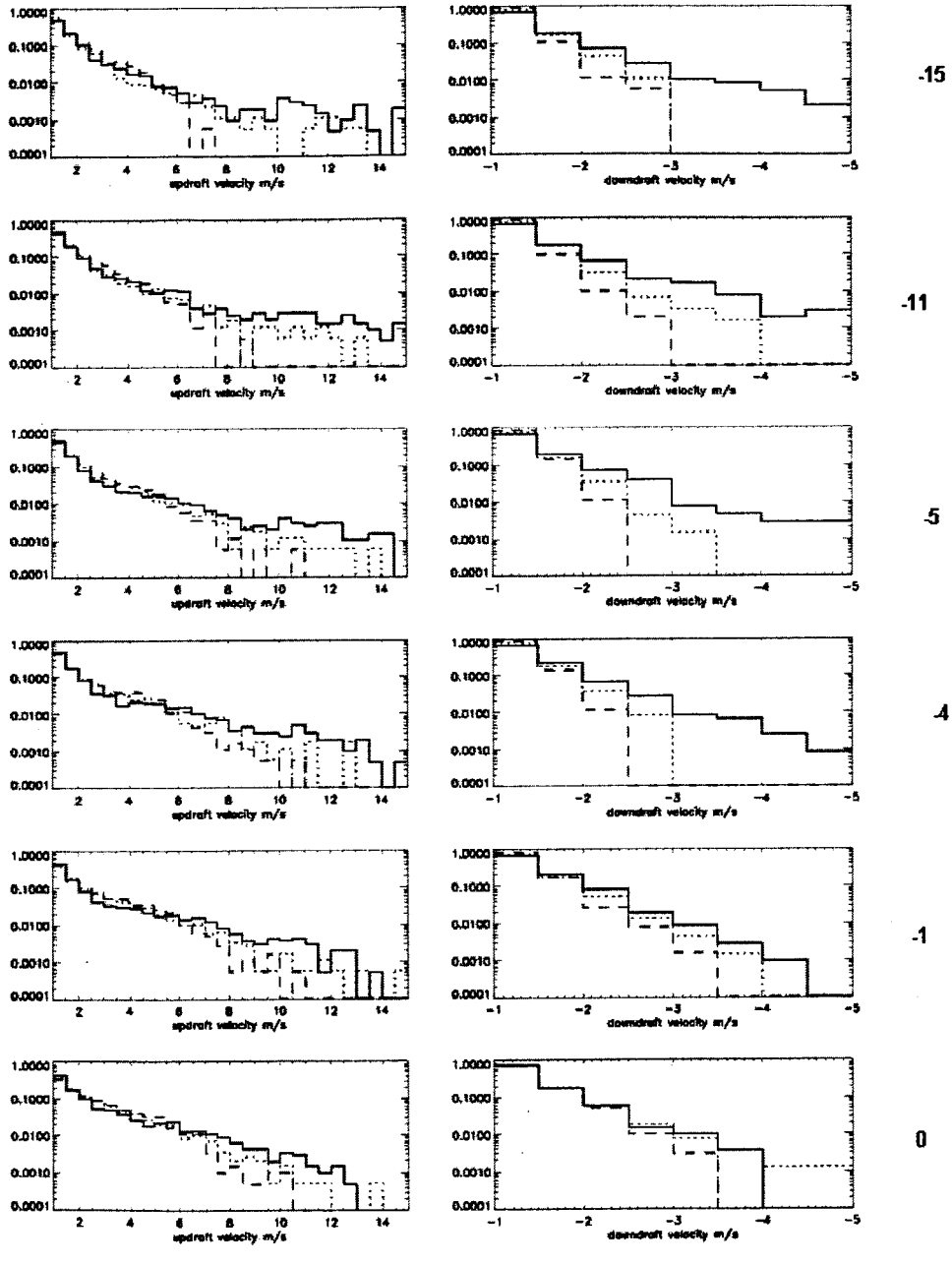

Figure 19: As in Fig. 18, except for simulations with varying representations of graupel fall speed: solid, original simulation; dashed, faster falling graupel; dotted, slower falling graupel.

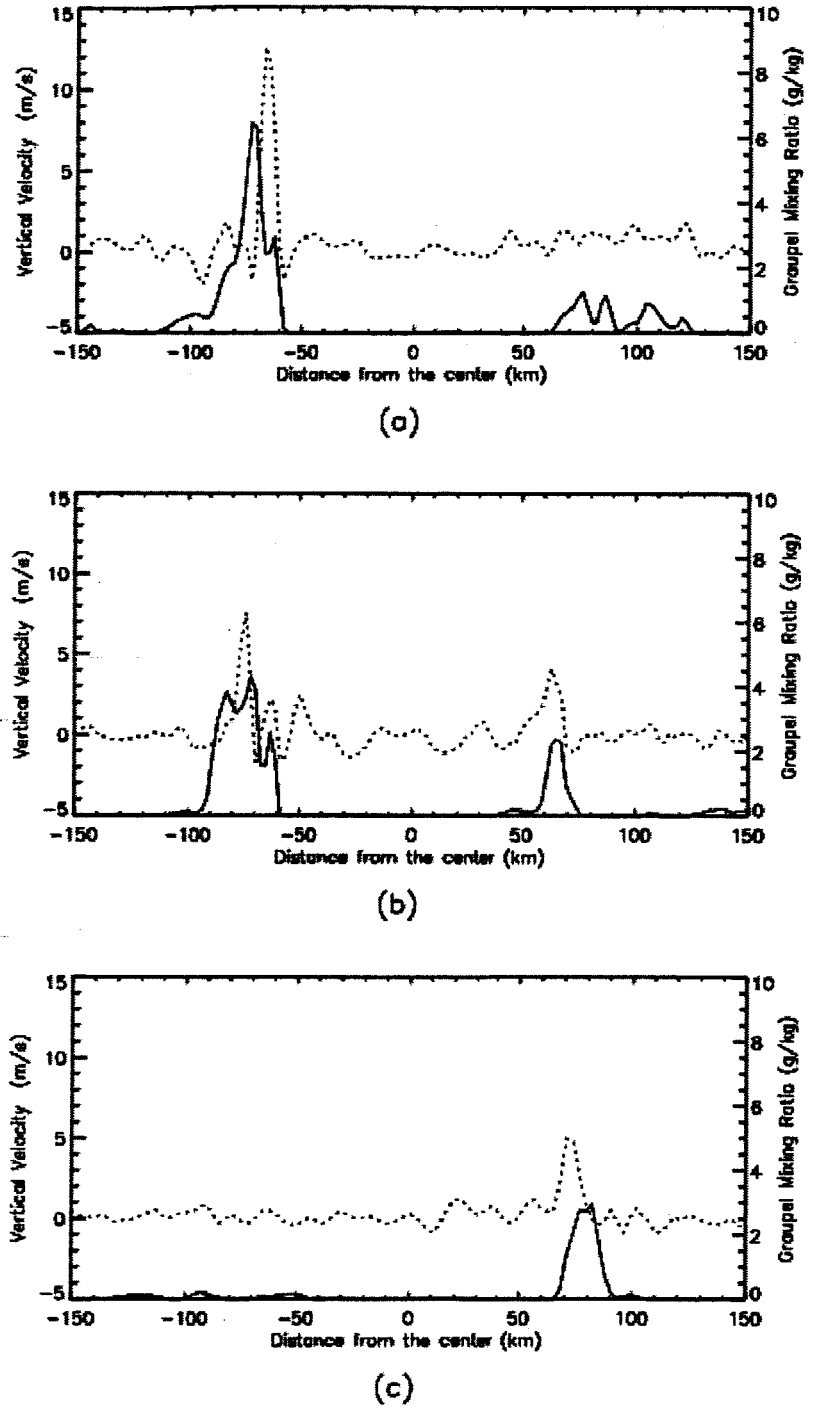

Figure 22: Plot of graupel mixing ratio and vertical velocity at temperature of –5°C for varying distance along a cross-section that cuts through the eye of the hurricane.

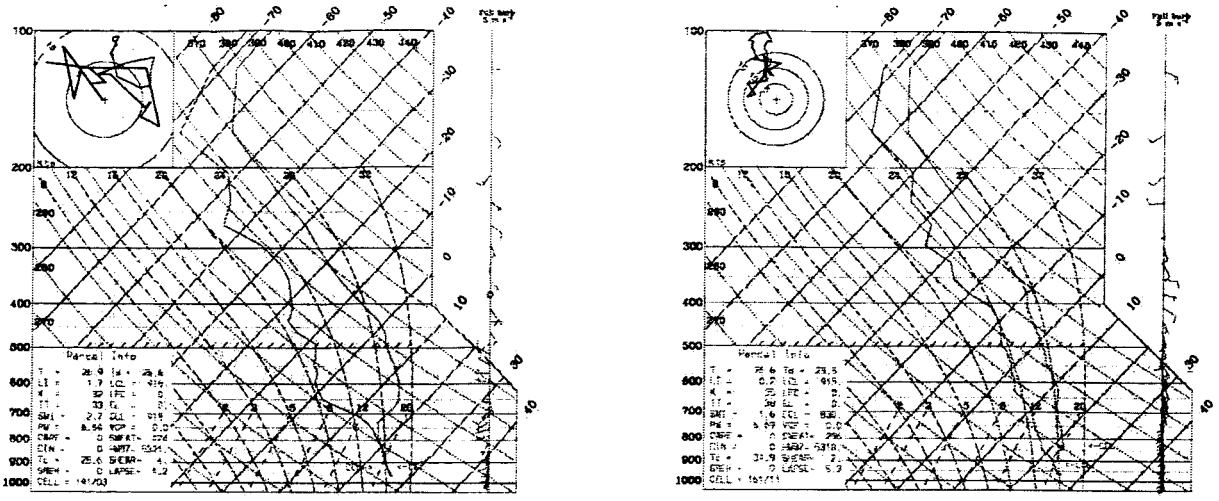

Figure 25: Vertical profile of temperature and dew-point temperature for model simulation using the new iterative condensation scheme.